NEUTRON RESONANCES IN SODIUM, ALUMINUM, AND POTASSIUM

by

A. Louis Toller

Date: Sept. 24, 1954

Approved:

Henry W. Newson
Eugene Gerling
L. W. Nordheim
H. W. Lewis
F. D. Drexel

A thesis

submitted in partial fulfillment of
the requirements for the degree
of Doctor of Philosophy in
the Graduate School of
Arts and Sciences
of
Duke University

1954

PREFACE

This thesis reports the construction of a cylindrical electrostatic analyzer, designed to improve the resolution of measurements of neutron cross-sections, and the results of such measurements on several light nuclei.

The work could not have been performed without the very patient guidance of Dr. H. W. Newson, the project director. I wish to thank Dr. R. M. Williamson, who supervised the construction of the analyzer, and Dr. J. H. Gibbons, whose collimation and detection equipment were used in making measurements. Both were ever ready to assist in trouble shooting when necessary, no matter what the time of day or night. The analysis of transmission experiments by Dr. Eugen Merzbacher and Bernard Chern was used in attempting to deduce certain properties of the resonances. Dr. Merzbacher was especially generous with his time in assisting in the calculations.

Mr. Robert Rackley aided in the construction of the electronic circuits used to govern the functioning of the analyzer. The members of the Duke Instrument Shop, under the direction of Mr. Milton Whitfield made many of the analyzer parts. Mr. S. A. Cox assembled the analyzer power supply. Mr. Fred Egli very ably kept all electronic circuits in working condition, and was helpful in the taking of data, particularly in the small hours of the morning. The friendly and cooperative spirit of the entire Van de Graaff group, who unstintingly gave of their time to assist in

taking data, made the work much less tedious than it might otherwise have been.

I wish to thank my family and Duke University, without whose financial assistance I could not have pursued my studies, and most of all, my wife, who so unselfishly, and cheerfully did without many of the ordinary comforts, in order that I might complete my studies.

The work described in this thesis was supported by the Atomic Energy Commission.

A.L.T.

CONTENTS

LIST OF FIGURES

NEUTRON RESONANCES IN SODIUM, ALUMINUM, AND POTASSIUM

INTRODUCTION

Most nuclear reactions, for experimental purposes, are produced by exposing a target containing the nuclei under investigation to a beam of nucleons (protons or neutrons) or light nuclei (deuterons, tritons, alpha particles). Any incident particle which, in passing through the sample, comes within range of the nuclear force exerted by a target nucleus, may or may not, react with that nucleus. If a nuclear reaction does occur, it may be one of several kinds. It may be elastic scattering, inelastic scattering, radiative capture, capture followed by emission of a particle which differs in kind from the initial projectile, or capture followed by emission of more than one particle or photon.

The probability that a specific one of these reactions will occur is a function of the type and state of the projectile, and of the type and state of the target nucleus. The probability that some reaction will occur is the sum of the probabilities for the specific reactions.

All these probabilities are expressed in terms of σ, the cross section for the reaction. Its definition[1] is:

$$\sigma = \frac{\text{number of events of given type per unit time per nucleus}}{\text{number of incident particles per unit area per unit time}}$$

The probability that some reaction will occur is called the total cross section. Cross sections are measured in units of barns, where one barn is defined to be 10^{-24} cm^2. The work reported in this thesis is concerned solely with total cross sections for neutron induced reactions. Neutron cross sections, as opposed to charged particle cross sections, may be measured conveniently by the transmission method, since neutrons are acted upon only by nuclear forces. Thus neutrons are removed from a beam only by nuclear reactions, and comparison of the number of neutrons incident upon a target with that passing through the target undeflected, gives a direct measure of the number of nuclear reactions taking place within the target.

The neutron was discovered by Chadwick[2] in 1932. In that same year, de Broglie and co-workers[3] performed experiments using a radon-beryllium neutron source. In 1933, Dunning and Pegram[4], using a much more powerful source of the same type, performed experiments on total neutron cross sections. In 1934 and 1935, Fermi et al[5,6] performed activation experiments using the same type of neutron source. In all these cases the neutron energy was very indefinite. Neutrons were classified as either "slow" or "fast." The one-body approximation, which had been applied so successfully to the study of atomic spectra was applied to the study of the nucleus. The incident projectile was

considered to move in the average field of the nucleus. In consequence of this line of reasoning, it was predicted that cross sections should be inversely proportional to the neutron velocity.

However, Dunning[7] in 1934 and Amaldi et al[6] in 1935 found anomalously high cross sections in some reactions induced by the more energetic group of neutrons. In 1935, Bethe[8] postulated that neutron cross sections were due to two factors, the 1/v contribution which followed from the Hartree approximation, and a second "phase" factor. This second factor accounted for the appearance of resonances. This theory further predicted that large capture cross-sections and large elastic scattering cross-sections should occur together.

In 1936, Breit and Wigner[9] advanced their more quantitative theory of resonance effects. This theory has been reformulated[10-14] and extended[15,16] several times. It has enjoyed remarkable success and, today, enjoys a position as the foundation upon which much of the subsequent theory has been built. The Breit-Wigner theory may be divided roughly into two parts: that dealing with isolated resonances, the one-level equations; and that concerned with many closely spaced levels, the many-level equations. In this thesis, we shall use the one-level equations exclusively.

It is, perhaps, fitting to mention here, that the Breit-Wigner theory, itself, rests upon a more fundamental base. That is the theory of the compound nucleus, advanced by Bohr[17] in 1936. In his theory, Bohr postulated that nuclear reactions could be divided into two steps. First, a compound nucleus is formed from the incident particle and the target nucleus. This

nucleus is always formed in an excited state, having as the excitation energy the binding and kinetic energies of the incident particles. The second step is the decay of the compound nucleus to a residual nucleus and a particle(s) or photon(s). The compound nucleus has a large number of possible energy levels, which may be classified into two groups. First, the decaying states (virtual levels), in which the total energy of the nucleons is slightly positive. By analogy with atoms, the decaying states should form a continuum. However, in nuclei, these states are discrete, and have a finite lifetime. Second, the continuum, where, as the name implies, to all intents and purposes, the energy levels are continuous. The boundary between the decaying states and the continuum is neither sharply defined, nor even fixed. As experimental techniques improve, it becomes possible to resolve energy levels which once were considered to belong in the continuum. Thus the upper limit of excitation energies in the decaying states moves constantly upward.

Bohr's compound nucleus theory has been quite successful in describing nuclear reactions. It too, can be divided into two parts. The first is that describing reactions induced by low, or medium, energy projectiles. In these cases, the incident particle brings only a small excitation energy into the compound nucleus. Consequently, there are only a few exit channels by which decay can take place. One of these is certainly the entrance channel. This situation leads to the appearance of resonances. The second division of the theory is that describing reactions induced by very high energy projectiles. In such re-

actions, the compound nucleus is highly excited, many channels for decay are open, and the probability of decay into the entrance channel is very low. This treatment predicts neutron cross-sections which are a smooth function of energy and exhibit neither sharp maxima nor sharp minima. Both regions of the energy spectrum are now under intensive investigation.

There is increasing evidence which indicates that the Bohr picture will require some modification. It is based on the belief that inter-nucleon reactions are strong and approximately equal. However, experimental evidence, dating as far back as 1917[18] indicates that there may, instead, be preferred configurations of nucleons. Numerous tabulations[19-23] have been made, and experiments performed[24-29] which demonstrate that nuclei containing certain "magic" numbers of neutrons or protons are more stable than others. This has led to the theory that nucleons form closed shells, much as atomic electrons do.[30] Such increased stability is indicated by anomalously wide spacing of energy levels--and therefore, of neutron resonances.

In the experiments described in this thesis, four different light nuclides were investigated. Of these, two contained questionably magic numbers of neutrons (Al^{27} and K^{39}) and two were magic in neither protons nor neutrons (Na^{23} and K^{41}). Transmission experiments in the resonance region were carried out in all cases, using a rather intense, yet highly analyzed beam of neutrons. It was expected that a number of resonances would be found in the total cross-sections. It was hoped that the peaks would be delineated sharply enough for us to assign level-widths

and J values to at least some of them, thus enabling us to estimate level spacings. It was further hoped that the information gathered, when coupled with that gleaned from similar experiments being carried on simultaneously in this laboratory, would shed substantial new light on the behavior of light nuclei. It is still not clear whether such possibly magic numbers as 10, 14, or 20 have an effect on neutron resonances.

Chapter I

APPARATUS

The apparatus used in these experiments consists of three chief components.

1. A Van de Graaff electrostatic generator.

2. A cylindrical electrostatic analyzer, similar to that in use at the University of Wisconsin,[31] constructed in this laboratory under the direction of Dr. R. M. Williamson.

3. Collimation and detection apparatus[32] constructed in this laboratory by Dr. J. H. Gibbons.

A beam of ionized particles is created in the r-f ion source of the Van de Graaff generator, and is accelerated through a relatively smooth voltage gradient, down the accelerator tube. This beam consists of protons, deuterons, various charged hydrogen molecules, plus any impurities which may be present in the hydrogen gas. A localized, intense magnetic field, at right angles to the path of the ion beam, effectively separates the various components in space. Thus a relatively pure proton beam may be

selected.

A certain degree of homogeneity in ion energy as well as in ion type is attained. However, the energy spread is of the order of .5% Thus, a 2 MEV proton beam would have a maximum energy uncertainty of approximately ±10 KEV. Obviously, any experiment performed with such a beam must have a correspondingly large energy uncertainty. Passing the proton beam through a cylindrical electrostatic analyzer reduces the energy spread without the loss of a prohibitive fraction of the beam.

The electrostatic analyzer consists of two conducting plates, kept at extremely steady potentials, and a slit system. (See Figures 1, 2, and 3) The plates are sections of concentric right cylinders. A uniform, and small, gap exists between the outer surface of the inner plate and the inner surface of the outer plate. These two surfaces are geometrically inverse with respect to the surface of radius a. The actual dimensions, in our geometry, are listed in Appendix A. An intense, approximately radial electric field is maintained in the gap between the plates. This field is directed toward the common axis of the plates.

If one assumes that the field is precisely radial, and cut off sharply at the ends of the analyzer plates, and that the proton motion takes place in a plane, it can be shown[31] that all protons of a given energy, which pass through a point in the object plane, will be focused into a point in the image plane. Herzog[33] has shown that the sharp cut-off of the electric field at the ends of the plates is a good approximation if ground

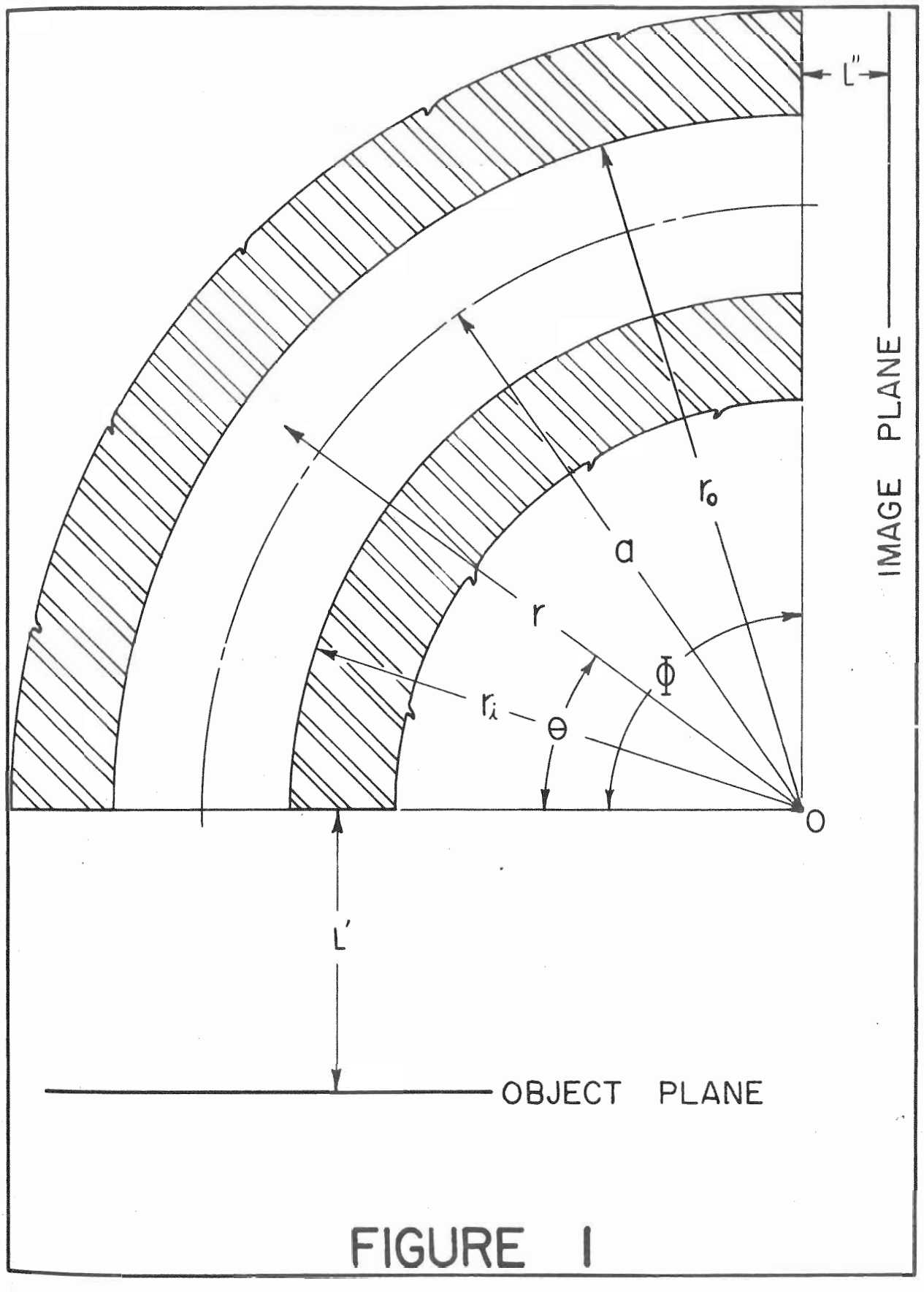

FIGURE 1

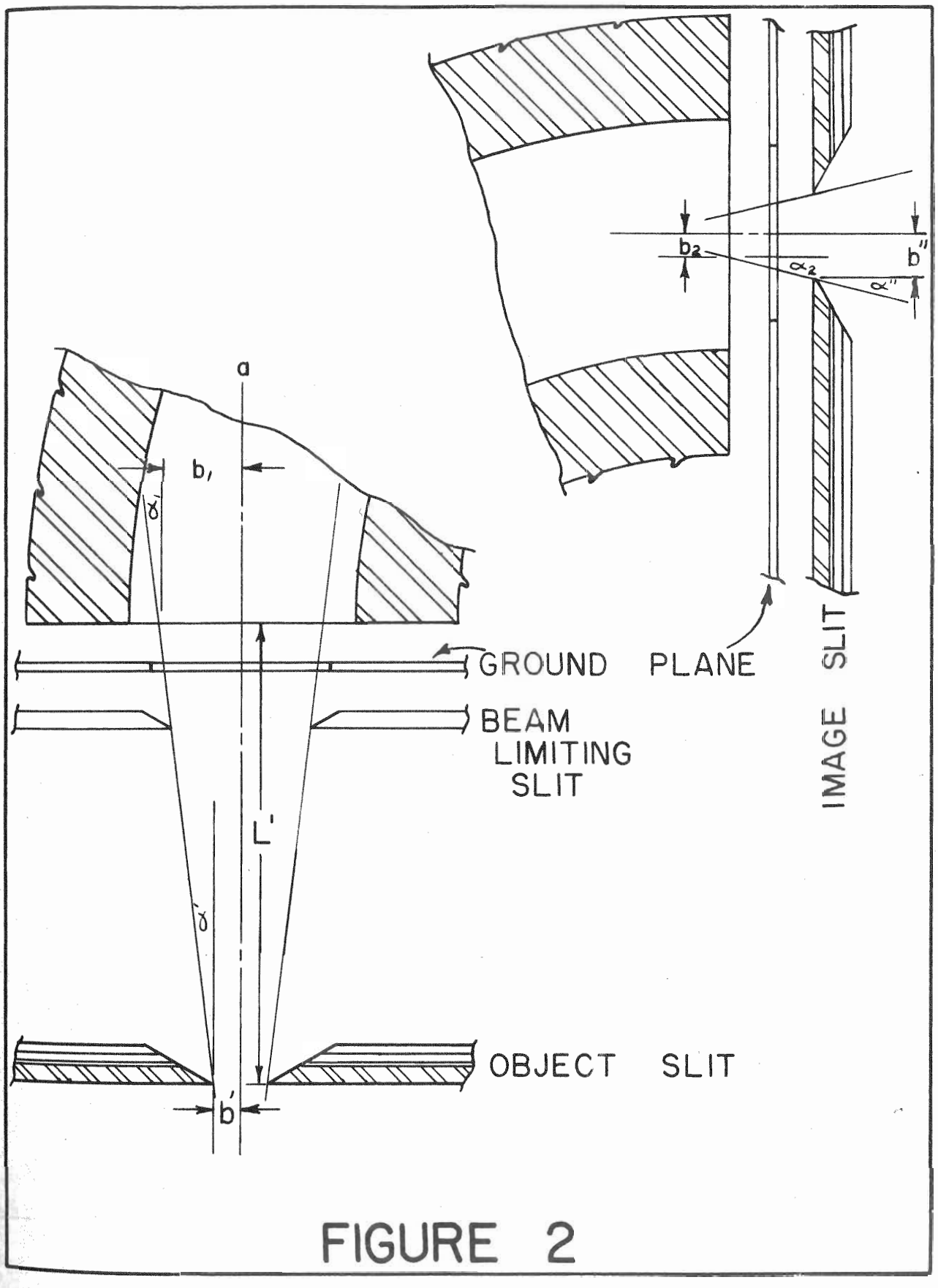
a
b1
α1
GROUND PLANE
BEAM LIMITING SLIT
L'
α'
b'
OBJECT SLIT
b2
α2
b''
α''
IMAGE SLIT

FIGURE 2

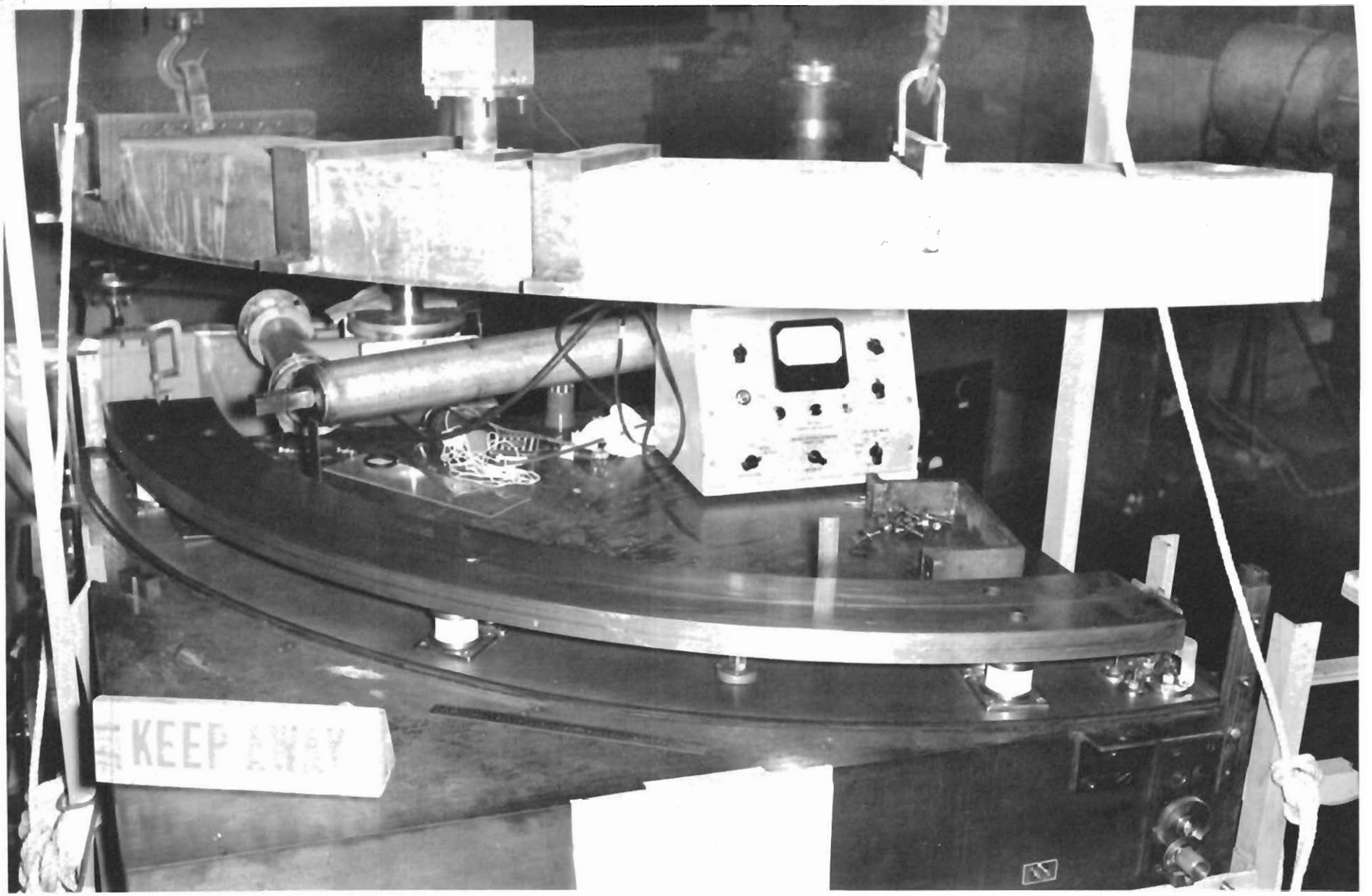

Figure 3

planes are inserted near the ends.

We make the following definitions:

$V'/2$ Potential of outer plate

$-V'/2$ Potential of inner plate

r_i Outer radius of inner plate

r_o Inner radius of outer plate

a mean radius; $a^2 = r_i r_o$; a is extended to include the tangents to the circle of radius a outside the plates.

V The potential through which a proton has fallen before entering the analyzer.

V_o That particular V such that a proton of energy eV_o, entering the analyzer tangent to the circle of radius a, will follow a circular path of that radius. V_o is a function of V'.

q $(V-V_o)/V_o$

L' Distance between object plane and entrance end of analyzer plates (object distance).

L" distance between exit end of analyzer plates and image plane (image distance).

Subscript 1 refers to events at the entrance end of the analyzer plates.

Subscript 2 refers to events at the exit end of the analyzer plates.

Primes refer to events in the object plane.

Double primes refer to events in the image plane.

b Distance between a proton and the circle of radius a. We use b_1, b_2, b', and b".

r Distance of a proton from the common axis, O.

α Angle between the velocity of a proton and the tangent to the circle of radius r.

w Slit width

Φ Angle subtended at the axis by the analyzer plates. In our geometry, Φ is 90 degrees.

In order that the equation defining the position of a proton in the image plane as a function of its position in the object plane and of its energy, be particularly simple and easy to remember, we define three constants of the instrument, which depend solely upon the fixed geometry of the analyzer.

f For non-relativistic cases, $f = (a/\sqrt{2}) \csc \sqrt{2}\,\Phi$
In our arrangement, f = 35.632"

g For non-relativistic cases, $g = (a/\sqrt{2}) \operatorname{ctn} \sqrt{2}\,\Phi$
In our geometry, g = - 21.585"

M Magnification of the instrument. $M = f/(g - L') = - .634$

Detailed analysis shows that, for non-relativistic protons, and to a first-order approximation:

$$b'' = (a/2)(1-M)q + Mb'$$

That is, all protons having the same fractional energy difference (q) from eV_o and having the same displacement (b') from a in the object plane, will have the same displacement (b") from a in the image plane.

For the moment, consider only those protons of energy eV_o, and assume that they are uniformly distributed in the object plane. We will then find them uniformly distributed in the image plane, over a distance -M times as large as the object slit opening. Furthermore, the proton passing through the object plane

at a emerges in the image plane at a. However, from the definition of M, we see that for $\Phi = 90^{\circ}$ and L' positive (both of which hold in our geometry), M is negative. If, therefore, we consider b positive for r > a, and negative for r < a, we observe that a proton with b' positive must have b" negative, and vice versa.

Now consider only those protons which have the same, positive $q = (V-V_o)/V_o$. We make the same assumption of uniform proton distribution in the object plane. That proton with the maximum b' will again have the minimum b". But the proton in the image plane will be displaced a distance (a/2)(1-M)q toward a more positive (or less negative) b". That proton with minimum b' will be displaced a like distance in the same direction, in the image plane. Thus, the image will still be -M times as large as the object, but it will be displaced by a distance proportional to q. If we describe q in arbitrary units, we may visualize the image as being composed of a superposition of component images, each with the same extent, -Mw', where w' is the object slit width, but displaced a distance proportional to q.

q = 0

q = -1 q = 1

q = -2 q = 2

q = -3 q = 3

q = -4 q = 4

A slit in the image plane, centered on a, may then be opened to such an extent as to exclude all protons with absolute value of q, written /q/, greater than a certain specified amount. If

we make the approximation that each energy included in the above diagram is equally probable, then the number of protons passing through the image slits will be proportional to the length of the line above. A slit opening such that all protons with q = 0 just get through, will exclude some of those with /q/ = 1, and exactly twice as many with /q/ = 2, etc. Thus, a plot of number of protons vs. q will be triangular, and symmetric about q = 0. This, then, is the distribution function of protons.

If, however, w" is greater than -Mw', then the distribution will be an isosceles trapezoid, since all the protons with /q/ less than or equal to some maximum value will pass through the image slits. A similar distribution will occur if the distance w" is less than -Mw'. In this case, however, even those protons with q = 0, will not all get through. Equal numbers of these and of protons with /q/ less than or equal to some specific value will be barred by the image slits. Therefore, the intensity will be diminished.

It is desirable to describe the performance of the analyzer in terms of the homogeneity of the proton beam impinging on the target. This is done in terms of R, the analyzer resolution. R is defined to be the reciprocal of q' where q' is so chosen that 75% of the protons passing through the image slit have $/q/ \leq /q'/$. For example, consider R = 2000 and V_o = 2 MEV. Then $q' = \pm 1/2000 = (V-V_o)/V_o$ and $V = V_o + V_o/2000$ = 2 MEV ± 1 KEV, and 75% of the protons have energies between 2.001 and 1.999 MEV.

Obviously, R is a function of the fixed analyzer geometry which determines the magnification, the object slit opening which,

together with M determines the size of each component image, and the image slit opening which determines just how much of each component image will be permitted to pass through.

A sample calculation of the resolution is made in Appendix B, and results are tabulated.

It can be shown that a linear relationship exists between the energy, eV_o, of the proton which travels through the analyzer in a circle of radius, a, and V', the potential difference between the plates. It turns out to be:

$$V_o = V'/2 \ln (r_o/r_i)$$

$$dV_o/dV' = 1/2 \ln (r_o/r_i)$$

For our geometry: $dV_o/dV' = 1/2 \ln(40.1840/40.0040) = 111$

Thus a change of only 10 volts across the analyzer plates results in a one kilovolt shift in the energy of the proton beam impinging on the target. Since, in operation, V' is of the order of 20 KEV, this means that the analyzer plate potentials must be kept constant within $\pm$ .05% in order that the proton energy be known within $\pm$ 1 KEV.

In order to obtain this high stability, an independent power supply[34] is used for the analyzer plates. A 400 cycle Leland generator, driven by a 3-phase induction motor is the initial source of power. Current is then passed through a degenerative regulator circuit, designed to minimize the effects of fast fluctuations. It then passes through a control circuit which acts as a stabilizer against slower changes and voltage drift. From here, power is fed to the primary of a high voltage transformer. The transformer output passes through a resistance-

capacitance filter, and then to the analyzer plates. A bleeder resistor is connected between the analyzer plates and ground, and taps are provided in order that a reference voltage may be tapped off. This reference voltage is then compared with the output of a potentiometer. Any difference in these two voltages is fed to a galvanometer-phototube amplifier. This amplified error signal is fed back to the control circuit (Henkel-Petree circuit) where it acts to change the input voltage to the primary of the high voltage transformer.

A detailed description of the power supply is given in Appendix C, and the operation of the control circuit is more fully described in Appendix D.

Figure 4 is a picture of the potentiometer and the front of the control chassis.

Figure 5 shows the galvanometer, with undeflected light. In the foreground is a meter which reads the proton current impinging on the lithium target.

Figure 6 is a picture of the analyzer power supply. One bleeder resistor stack is prominently displayed in the foreground.

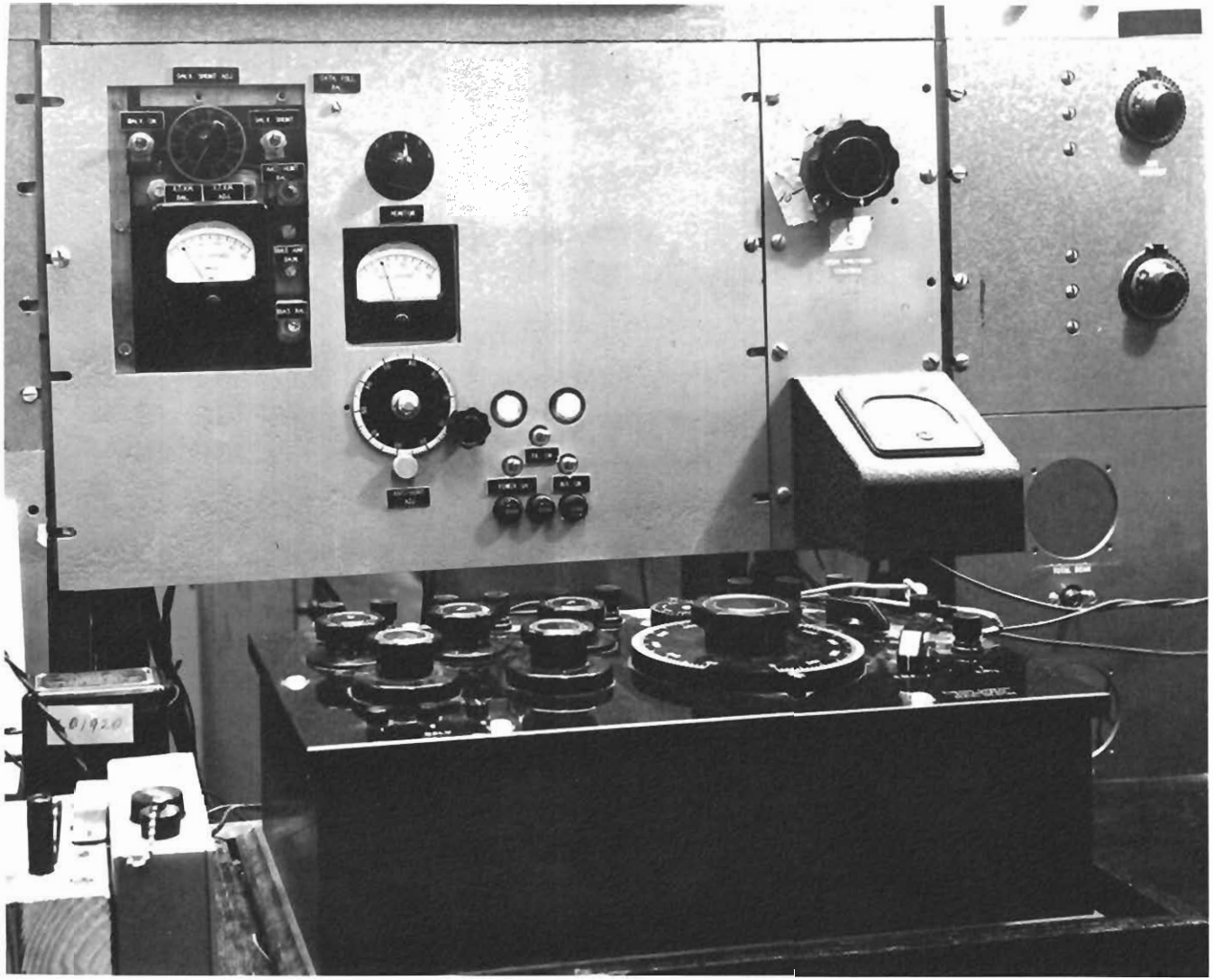

Figure 4

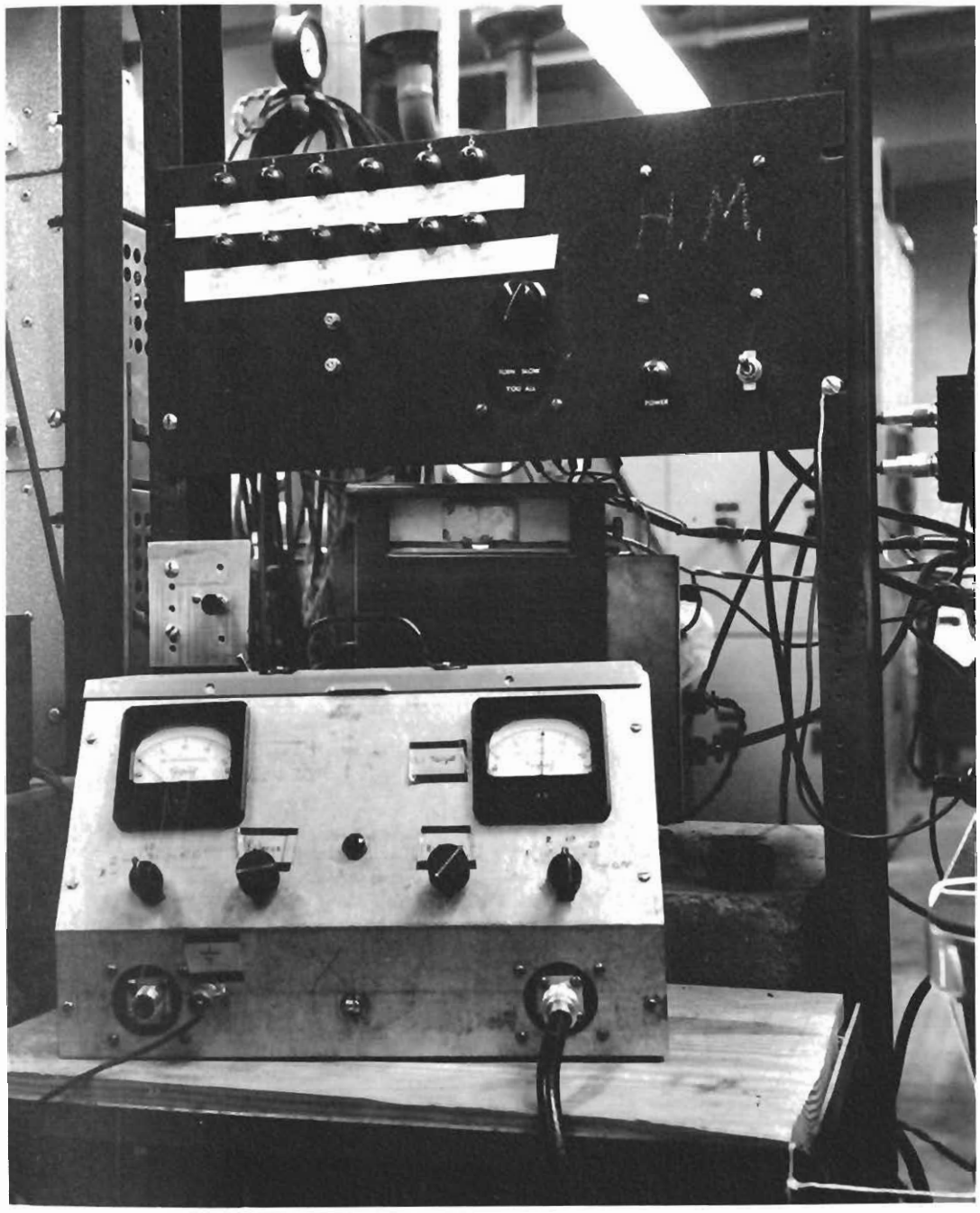

Figure 5

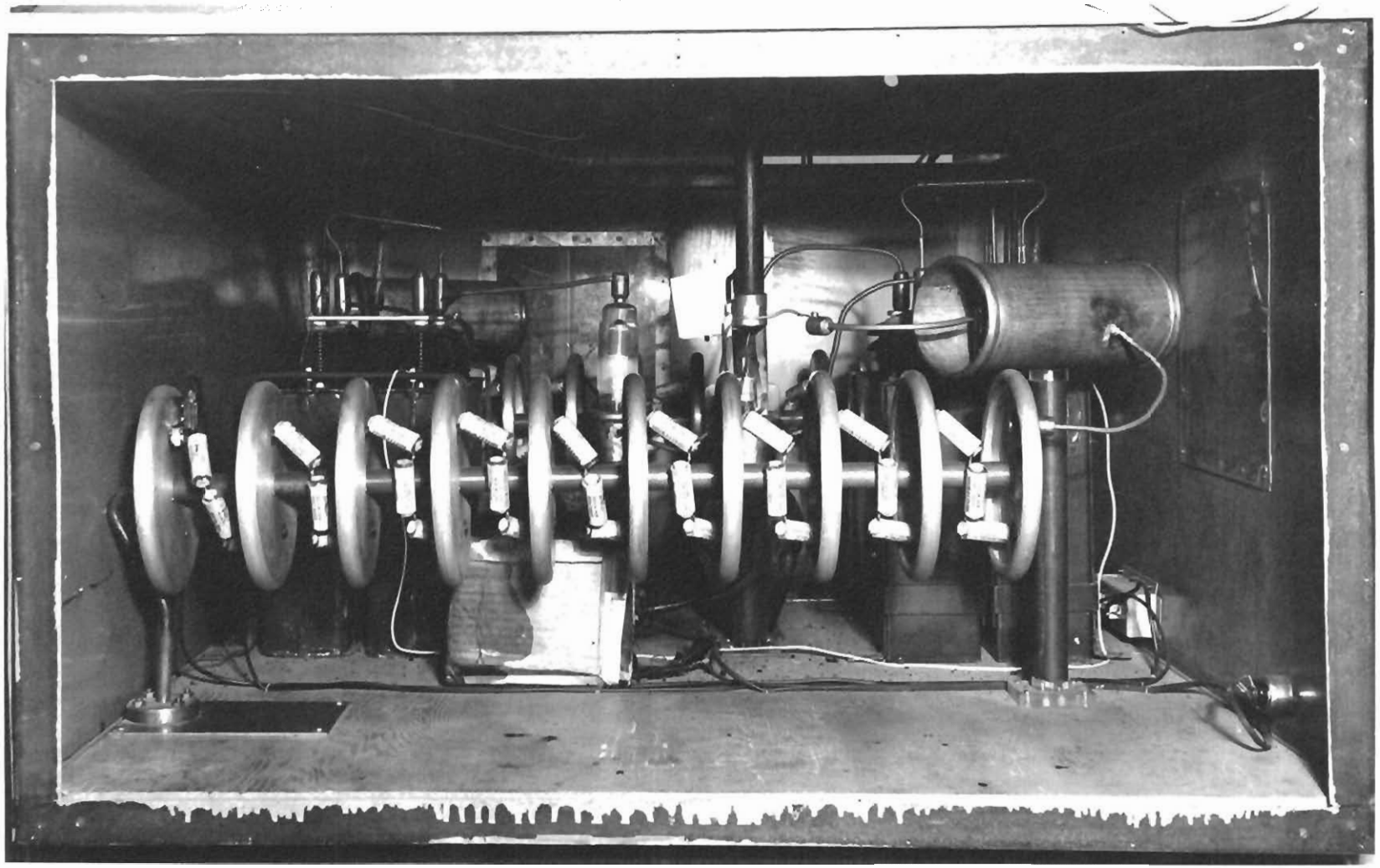

Figure 6

Chapter II

PROCEDURE

Total neutron cross sections were measured by the transmission method. The specific method used has been described[35] in detail elsewhere. Briefly, protons emerging from the electrostatic analyzer impinge on a .002" platinum end cap upon which a layer of lithium has been evaporated. Neutrons from the Li(p,n) reaction pass down a shielded collimator, making an angle of 122 degrees with the proton beam, and are counted. Counts were taken twice with no sample in the beam and twice with the target under investigation intercepting the neutron beam. This was done to minimize the probability of accepting incorrect counts which might have been caused by any of a number of transient causes.

Al^{27} was the first of the nuclides investigated. Preparation of the samples presented no problem. 2S aluminum of commercial grade was simply machined to the desired dimensions. Various thicknesses were tried, but the bulk of the data was taken with

two targets. One contained 2.163×10^{23} atoms/cm^2 and the other contained $.4337 \times 10^{23}$ atoms/cm^2.

The second nuclide investigated was Na^{23}. Two samples of metallic sodium were used. Due to the rapid corrosion of sodium when exposed to air, the samples were encased in airtight containers, and their entire preparation took place under oil or ether. The containers were of two types, depending upon the thickness of the sample. For the thicker, the container consisted of two thin-walled steel cylinders, each closed at one end with .005" silver. Each had a threaded flange at its open end such that the two cylinders could be screwed together. A vacuum seal was maintained by an "O" ring between the flanges. One of the cylinders had a small "pump out" tube.

The metallic sodium was furnished in approximately cylindrical form. It was pressed by hand, under mineral oil, using the smooth end of a steel cylinder, to a thickness just a little larger than that desired. A "cookie cutter" was then used, again with only hand pressure required, to cut the sodium to the proper diameter. The process was repeated, this time pressing to the desired thickness and again using the cookie cutter to get the final sample. The oil was removed by successive baths in dilute mixtures of dried alcohol in dried ether. No precise measure of the ratio of alcohol to ether was made, but the baths were prepared as follows. Approximately 10cc of alcohol were diluted with 250cc of ether. About 10cc of this mixture was then added to 250cc of ether. In turn about 10cc of this mixture was added to 250cc of ether. The process was repeated until four

baths were ready, the last containing about 500cc of mixture. This method was necessary because it was found that ether alone did not inhibit the formation of the oxide, while anything but a very dilute mixture of alcohol attacked the sodium vigorously. The sample was dipped into each bath in turn, and removed immediately, starting with the least dilute mixture. It was permitted to remain only in the last for any appreciable time.

The container was submerged in the last bath, and loading took place beneath the surface. A Welch vacuum pump was connected to the pump-out tube, and started pumping before the container was removed from the bath. Pumping continued for 24 hours, after which the copper pump-out tube was crimped in several places, then cut off and immediately plunged into molten solder.

The thinner of the two sodium samples did not permit enough depth in the container to enable the same type to be used. Instead, this container consisted of two doughnut-shaped, flat steel discs. The center hole of each disc was sealed at one end with .005" silver. Each disc was .5715 cm. thick, since that was the sample thickness desired. The discs were fastened together by four screws, and an "O" ring made the joint air-tight. The discs were joined in such a fashion as to leave just .5715 cm. depth for the sample. I.E. one disc actually contained the sample, while the other served merely as a cover. A copper pump-out tube in the former, made it possible to pump out residual gases after the container was sealed. The procedure for preparing and loading this sample was the same as that described above.

The thick sodium sample contained 4.839×10^{22} atoms/cm^2. The thin sodium sample contained 1.452×10^{22} atoms/cm^2.

In investigating the properties of potassium, both the natural metal and a sample of KCl,* enriched in K^{41} were used. Three different thicknesses of natural potassium were used. One contained 6.229×10^{22} atoms/cm^2; the second contained 4.611×10^{22} atoms/cm^2; and the third contained 1.578×10^{22} atoms/cm^2. The samples were prepared in the same manner as were the sodium samples, described above. The thinnest used a container similar to that used for the thinner sodium sample. However, in this case, the sample was 1.1913 cm. thick, so that it could be contained partially in each disc. The other two samples used containers just like that which housed the thick sodium sample.

The KCl was furnished in powdered form. Due to the small quantity available, the sample was pressed in a small die of rectangular cross-section. It was completely sealed in .005" silver, immediately after being pressed. This sample contained 1.097×10^{22} K atoms/cm^2. Since it also contained that same number of chlorine atoms/cm^2, and since the chlorine nucleus also exhibits resonances in the region under investigation, it was desirable to "balance out" the chlorine. Thus, a second sample (hexachloroethane, $C\,Cl_3\,C\,Cl_3$) was prepared, having precisely the same number of chlorine atoms/cm^2. This sample, too, was sealed in .005" silver. The transmission ratio was then

---

*Obtained on loan from the Isotopes Division of the Atomic Energy Commission. Prepared by C. P. Keim and coworkers at Oak Ridge National Laboratories.

taken to be the number of neutrons counted after passing through the KCl sample divided by that counted after passing the beam through the $C Cl_3$ $C Cl_3$ sample. This eliminated the chlorine cross-section from the calculation, substituting instead, the carbon, for which the cross-section in this region is well-known, and quite constant.

Neutrons passing through those samples which were sealed in containers, were also required to pass through .010" of silver. Rather than correct for this in the calculations, a .010" silver sample was also prepared, and the beam was passed through this sample to give the "out" count. This was not necessary in the case of the aluminum samples. At times two or more samples were being run simultaneously. Rather than take two separate "out" counts, either the silver or an actual "out" was used, whichever was more convenient. In such cases, the data were corrected to take into account the extra (or missing) .010" of silver.

The energy range covered was not the same in all cases. The aluminum was run from 0 - 160 KEV. The natural potassium was run from 0-320 KEV. The K^{41} sample was run from 0-120 KEV. The sodium was run from 0-160 KEV.

Chapter III

RESULTS

The results of these experiments are shown graphically in Figures 7 through 11. Experimental cross-sections, in barns, are plotted against neutron energies in kilovolts. Apparent cross-sections were calculated from the well-known equation:

$$N = N_o \exp(\Sigma_i \; n_i \; \sigma_i),$$

where N is the number of neutrons counted after the beam has passed through the target, N_o is the number of neutrons incident upon the target, n_i is the number per square centimeter of nuclei of type i, and σ_i is the total neutron cross-section of nuclei of type i. Due to imperfect resolution, this equation does not quite agree with experimental conditions. However, in cross-section work, it is the custom to ignore this unpalatable fact.

A theoretical relationship has been derived[36] between the width of a nuclear energy level, the spin of the compound nucleus,

and the area between the transmission curve (over the dip) and the line representing 100% transmission. This area analysis has been applied to several of the resonances found. To be most effective, this analysis requires that two different target thicknesses be run at the same time, one being much thicker than the other. In our experimental arrangement, however, there is a fixed upper limit to the thickness of targets. This limit is such that, in the cases of sodium, aluminum, and potassium there was not sufficient difference between the thick and thin samples to make optimum use of this analysis.

However, an alternative method may be applied when only one target thickness is used. Briefly, one plots the transmission, T, against neutron energy in KEV, extending the abscissa as far as possible on both sides of the resonance energy, E_o, without including the effects of adjacent resonances. He next selects various energies, d (measured in KEV), such that 2d is larger than the expected width, Γ. The area between the transmission curve, the line $T = 1$, and the ordinates at $E_o \pm d$, is then measured (in kilovolts) for various values of d. A Γ is calculated in each case. It is expected that, as d increases, the value of Γ should approach a fixed value. This is the correct value. In many cases, due to the proximity of other resonances, it is impossible to extend the wings of the curve far enough to get a good determination of Γ. However, the order of magnitude is usually ascertained.

Frequently, the area analysis does not distinguish between possible spin states of the compound nucleus. This distinction

may sometimes be made by applying the several possible Γ 's to a "peak height" analysis.[36] In this case, λ , the standard deviation of the assumed Gaussian distribution of neutrons is calculated for each Γ . λ may also be calculated from the geometry of the analyzer, and the lithium target thickness. Actually, a lower limit to λ is calculated by assuming an infinitely thin target. A Γ which leads to a λ less than this lower limit is eliminated, thus eliminating the corresponding spin.

In Figure 7, which shows the variation of neutron cross-section with neutron energy, two ordinate scales are used. The scale on the right refers to points plotted x; that on the left refers to points plotted with the conventional dot.

Only two resonances were found between zero and 160 KEV. The first was at 3.25 KEV, in agreement with earlier reports.[37] It appears to be quite narrow, and its peak height, measured with the thin sodium sample reached 62 barns. No analysis was carried out on this peak, since it was felt that the shape of the resonance and its low energy precluded the possibility of reliable results.

A second resonance was found at 53.5 KEV. It is not very strong, measuring only nine barns at the peak. There is no evidence of an interference dip on the low energy side of the peak, so presumably this is not an s resonance. However, Selove[37] found no dip before the 3.25 KEV peak which is almost certainly an s resonance. Consequently, this possibility cannot be definitely eliminated.

Area analysis of this peak using both thick and thin samples does not distinguish between possible spin states. However, it gives the order of magnitude of the width, Γ, which turns out to be approximately .7 KEV. Peak height analysis on the thick target also failed to select a spin. However, when the peak height analysis was applied to the thin sodium target, two different λ's were calculated for the neutron distribution function. These were 1.5 KEV for J = 2 and .9 KEV for J = 1. The minimum possible λ calculated from the experimental arrangement was .75 KEV. Since this calculation is based on an infinitely thin lithium target, it seems that the second experimental value is too low, and a very tentative assignment of J = 2, is made.

Sodium is not unlike chlorine[35] and phosphorus[38] in that it shows very few resonances below 100 KEV, certainly few of any strength. Thus s resonances are spaced at least 100 KEV apart.

The aluminum curve displays four prominent peaks between 0 and 160 KEV. The first is at 38 KEV. A definite minimum appears at 28 KEV, indicating that this is an s resonance. An area analysis was made for both target thicknesses, with the following results:

d (KEV)	J = 3		J = 2	
	Γ(KEV) thin sample	Γ(KEV) thick sample	Γ(KEV) thin sample	Γ(KEV) thick sample
1	.4	.4	.6	1.8
2	.8	.8	1.1	3.4
3	1.0	1.2	1.4	4.5
4	1.1	1.4	1.6	5.2
5	1.2	1.6	1.6	5.5

These results favor the choice of J = 3 and Γ = 1.7 KEV. This is further substantiated by peak height analysis. This analysis, in the case of the thick sample does not distinguish between the J values. However, for the thin sample, a value of Γ = 7.2 KEV is calculated for J = 2, while Γ = 2.7 KEV appears for J = 3. The minimum Γ is .6 KEV. It appears that 7.2 KEV is much too high. Therefore, again J = 3 emerges as the more likely choice.

A second peak in the aluminum curve appears at 90 KEV. Although no prominent dip appears just below this energy, this may be due to the proximity of the 38 KEV resonance. In any event the curve falls low enough to make it appear that this too is an s resonance. Area analysis on both thicknesses of aluminum gives the following results:

d (KEV)	J = 3		J = 2	
	Γ(KEV) thin sample	Γ(KEV) thick sample	Γ(KEV) thin sample	Γ(KEV) thick sample
1	1.4	1	4.1	1.5
2	2.8	2	8.2	2.9
3	4.0	3	11.5	4.1
4	5.3	3.7	13.3	5.1
5	6.2	4.7	14.5	6.4
6	6.9	5.3	14.7	7.3
7	7.4	5.9	14.5	8.1
8	7.9	6.2	14.2	8.3
9	7.9	6.4	13.5	8.5
10	8.0	6.5	13.2	8.6

Again, better agreement is reached if one assumes J = 3.

Peak height analysis makes no selection of J for either the thin or the thick sample.

A third peak appears at 120 KEV. However, it is believed that this is simply the sum of the effects of the resonances on each side of this peak, rather than representing an energy level. Therefore, no attempt at analysis has been made.

A fourth peak appears at 158 KEV. This actually appears to be an unresolved double peak.

Compared to sodium, fluorine, phosphorus, and chlorine^{35}, aluminum is unusual in having so many strong peaks at low energies. Apparently, the s resonances are spaced more closely in the case of aluminum.

Figures 10 and 11 show the neutron cross-sections of K^{41} and K^{39} respectively, from 0 - 120 KEV. The peak heights make it appear that the resonances in K^{41} are stronger than those in K^{39}. It must be remembered, however, that the K^{39} sample is much thicker than the K^{41} sample, which has the effect of depressing the peak heights of the former. In each case, seven peaks are counted between zero and 80 KEV, indicating a spacing of approximately 20 KEV per J value. A prominent interference dip appears just before the 43 KEV peak in K^{39}. Other than that, however, the close spacing of the levels makes it impossible to identify any interference dips which may be present.

Many points in Figure 11 fall below zero. This is probably due to the compensating hexachloroethane sample being a little too thick.

Both isotopes show resonances at 10, 23, 58, 96, and 110 KEV.

K^{39} displays other peaks at 29, 43, 68.5, and 87 KEV.

K^{41} has other resonances at 5, 17, 39, and 80 KEV.

Of the K^{41} peaks, only that at 39 KEV was analyzed. The results show a slight preference for $J = 1$ and $\Gamma = .9$ KEV rather than $J = 2$. However, this assignment is quite tentative, since there is but little to choose between the two results.

The peaks at 43, 58, and 68.5 KEV in K^{39} were analyzed. However, only one sample thickness was used, and the results did not distinguish clearly between possible J values. Using the average value, $g = 1/2$, it was possible to determine the orders of magnitude of the Γ's. The width of the 43 KEV resonance appears to be approximately .3 KEV, while that of the 58 KEV peak is approximately .6 KEV. The width of the 68.5 KEV resonance is approximately .8 KEV.

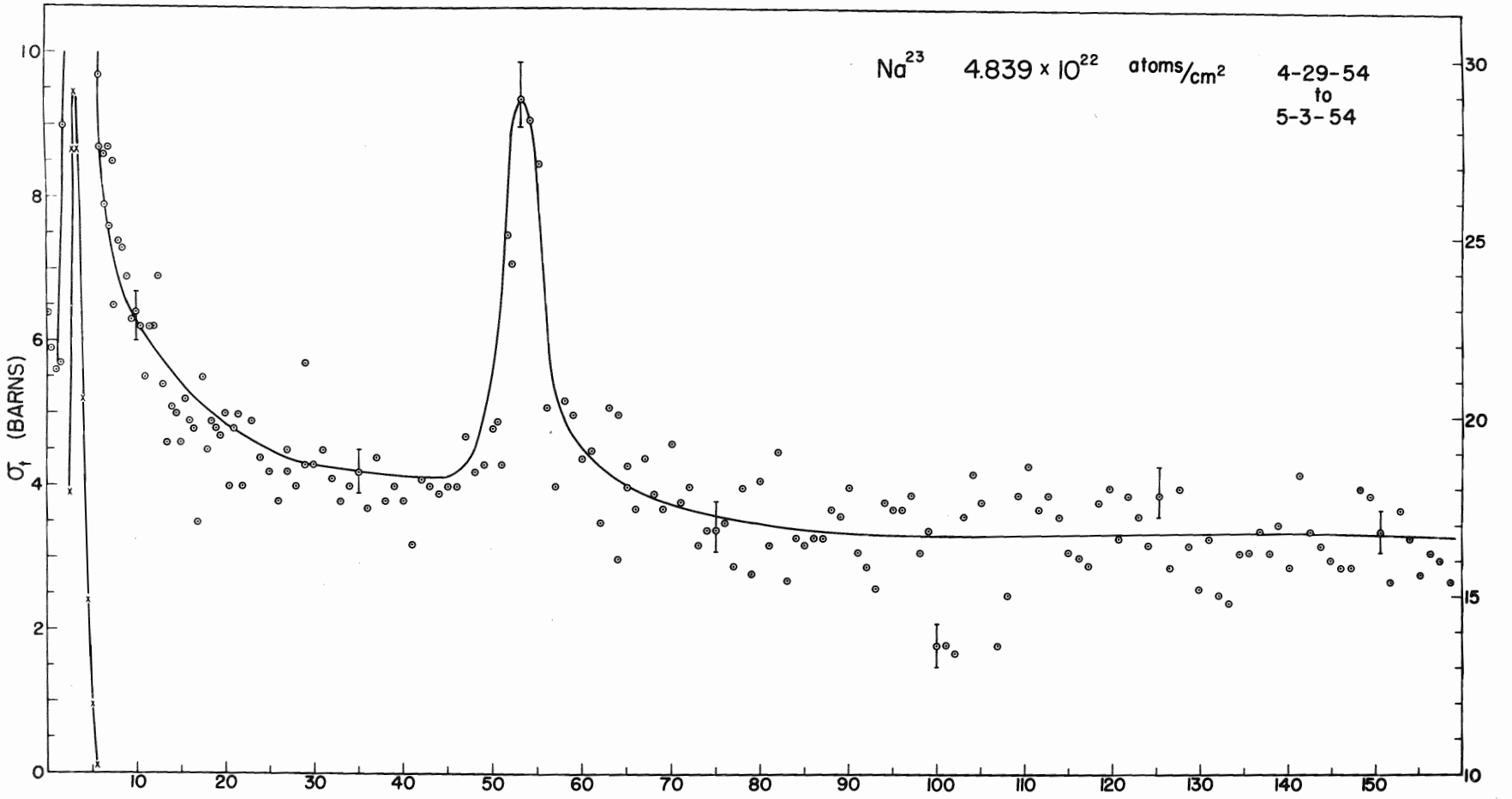
Na^{23} 4.839×10^{22} atoms/cm^2
4-29-54
to
5-3-54
σ_t (BARNS)
E_n (KEV)
0
2
4
6
8
10
10
15
20
25
30
10
20
30
40
50
60
70
80
90
100
110
120
130
140
150

FIGURE 7

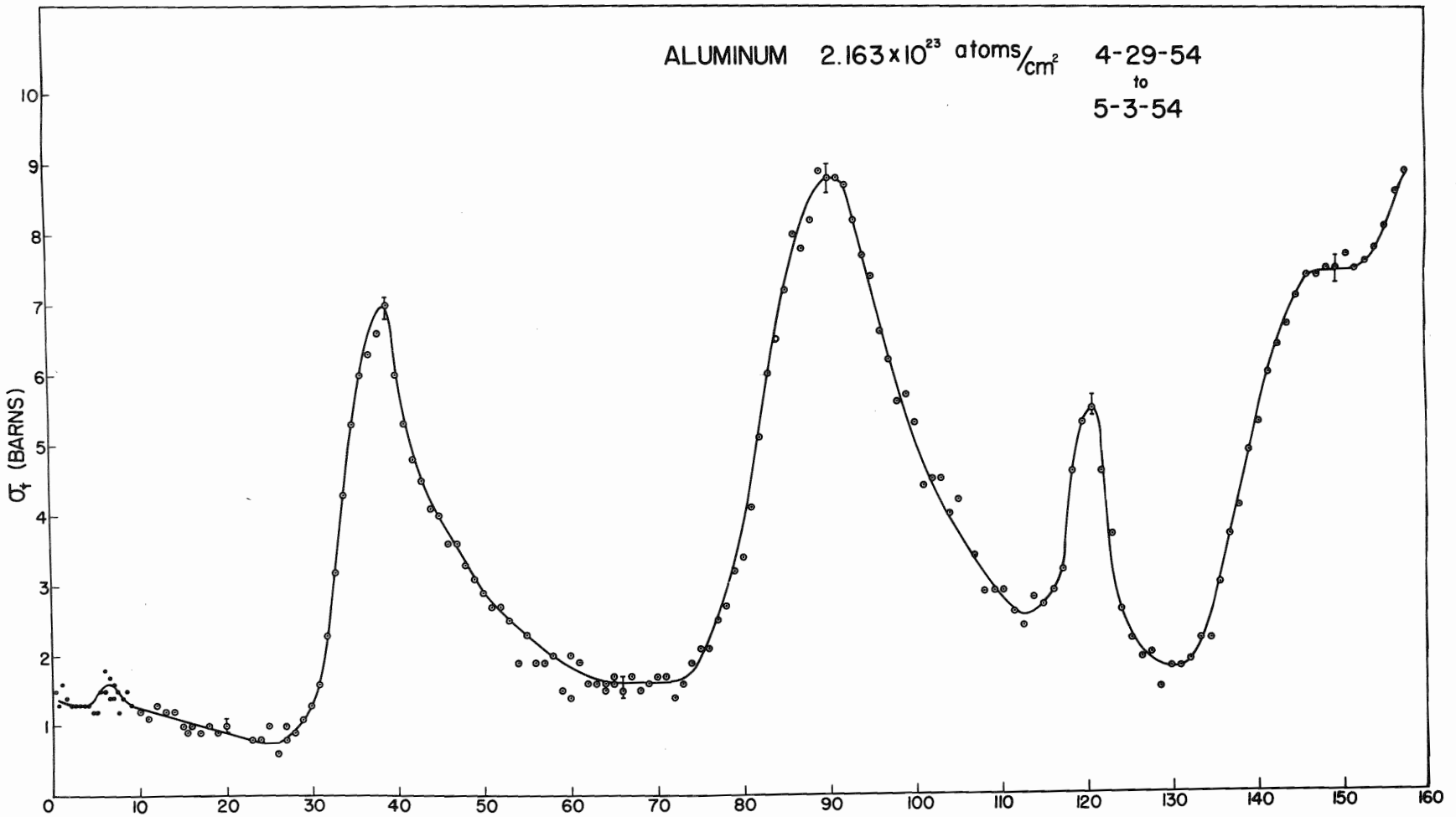
ALUMINUM 2.163 x 10^23 atoms/cm^2 4-29-54 to 5-3-54
σf (BARNS)
En (KEV)
0
10
20
30
40
50
60
70
80
90
100
110
120
130
140
150
160
1
2
3
4
5
6
7
8
9
10

FIGURE 8

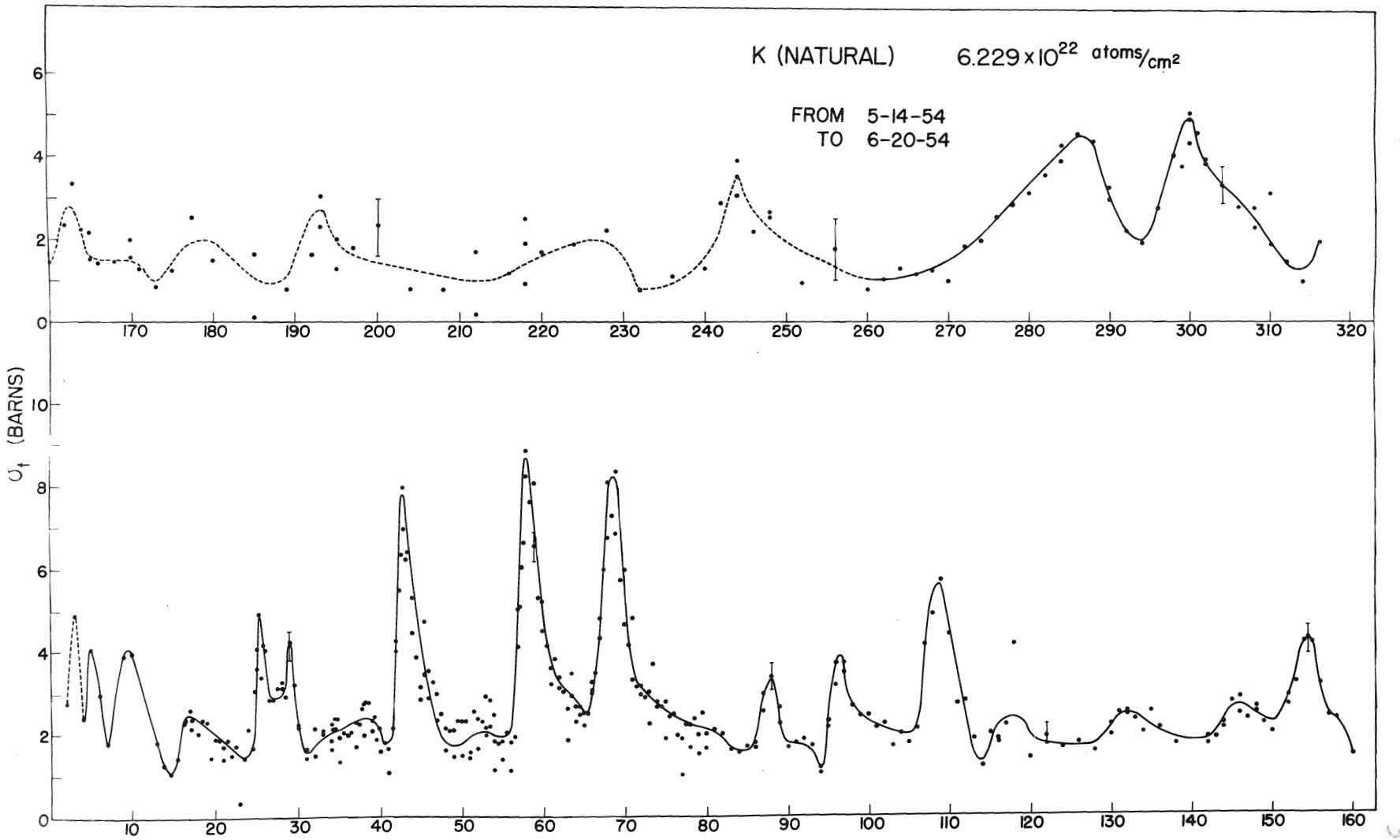
K (NATURAL) 6.229 x 10^22 atoms/cm²
FROM 5-14-54
TO 6-20-54
σt (BARNS)
En (KEV)

FIGURE 9

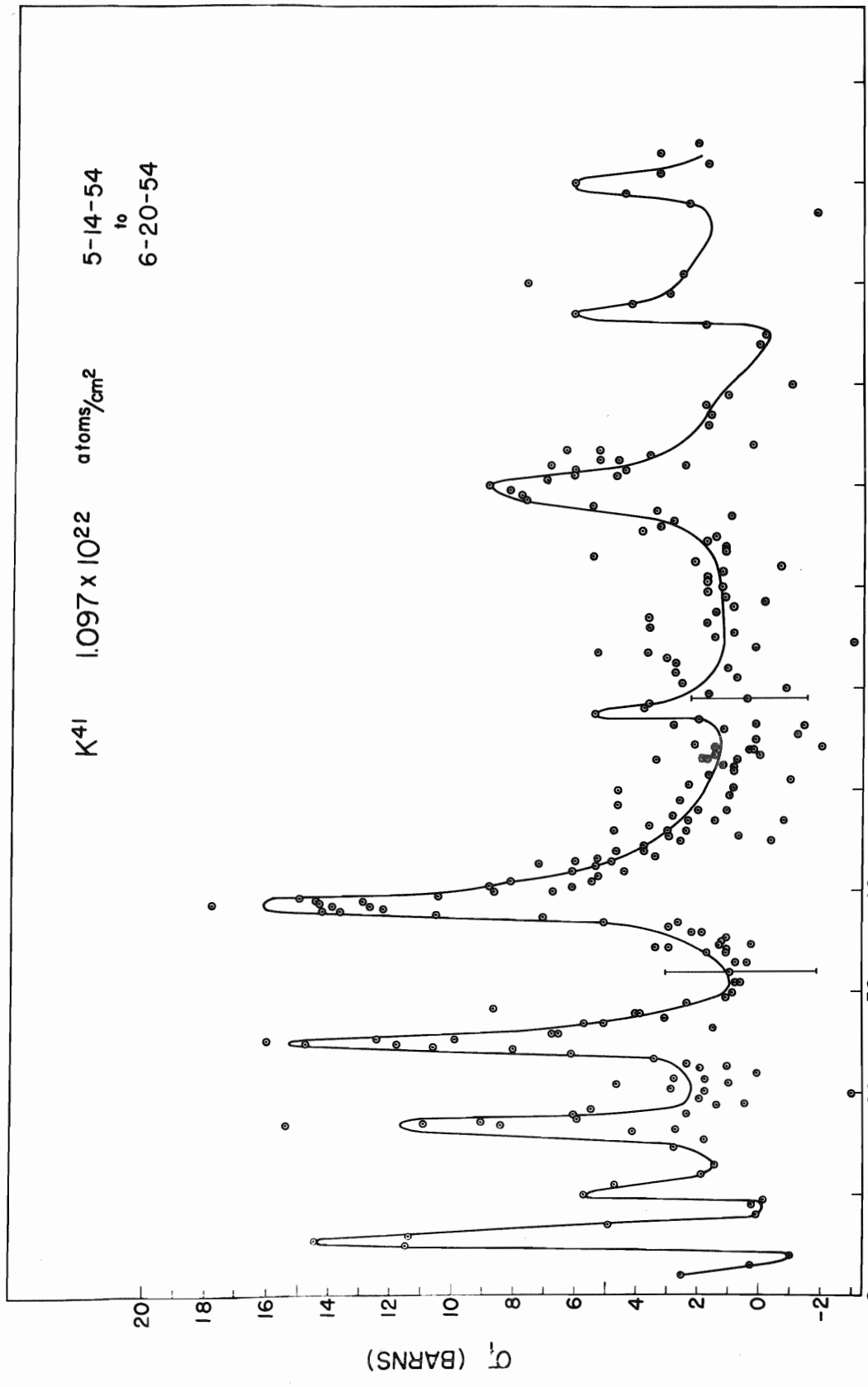

FIGURE 10

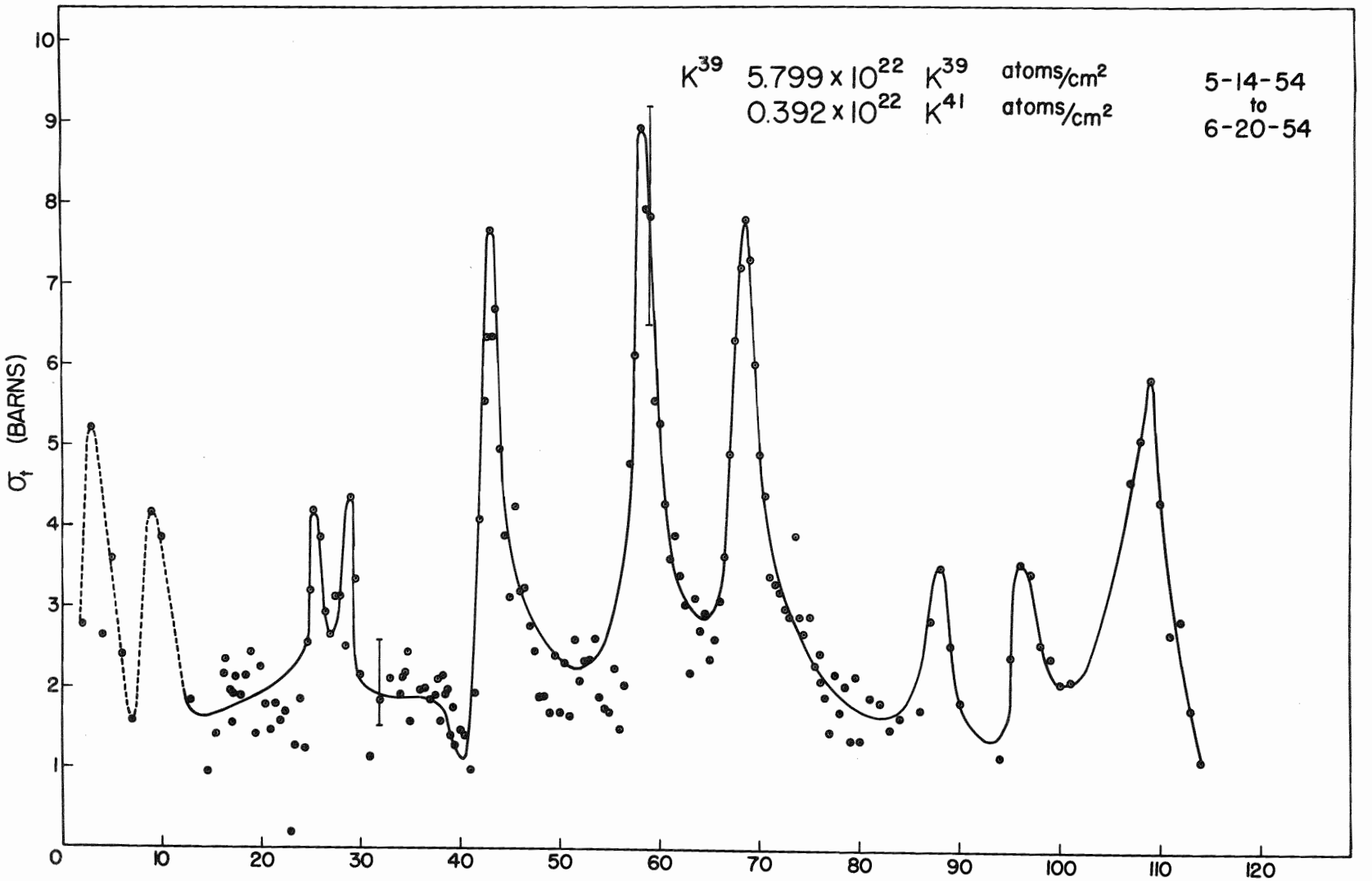
K^{39} 5.799×10^{22} K^{39} atoms/cm²
0.392×10^{22} K^{41} atoms/cm²
5-14-54
to
6-20-54
σ_t (BARNS)
E_n (KEV)
0
1
2
3
4
5
6
7
8
9
10
10
20
30
40
50
60
70
80
90
100
110
120

FIGURE 11

APPENDICES

Appendix A

PHYSICAL DESCRIPTION OF ELECTROSTATIC ANALYZER

The analyzer plates are made of steel, 1.5" x 3" in cross-section. The important radii are 40.0040" and 40.1840". They subtend an angle of 90 degrees at their common axis. The plates are mounted on a 4' x 4' Goodman, cast iron surface plate, and each is separated from it by three Mykroy insulating cylinders, 1.5" tall and 2.5" in diameter. The supports are spaced 10 degrees, 45 degrees, and 80 degrees from either end. Oversize holes are drilled in the plates over the 10 degree and 80 degree supports. Steel disks are bonded to the upper surfaces of these insulators and the plates are bolted to these disks. The oversize holes permit a certain flexibility in the final plate adjustments.

About .25" from each end of the analyzer plates, a grounded aluminum, fixed slit is located. An adjustable, beam-limiting slit is situated one inch from the entrance to the gap between the plates, and a similar image slit is provided one inch from

the exit end. The variable object slit is located 34.631" from the entrance end of the analyzer plates.

A welded cover, made of .75" 2S aluminum, fits down over the analyzer plates, and all the slits except the object slit. A rubber gasket between the cover and the surface plate makes a vacuum seal. Two viewing ports, covered with lucite, are provided, each in the top of the cover, so located that the slits may be seen from them. An ion gauge is situated at the midpoint of the upper surface of the cover. At each end there is, of course, an opening to permit passage of the proton beam without interference.

The analyzer has its own pumping system, consisting of a fore pump and a mercury diffusion pump, located at the exit end of the plates.

The Goodman plate forms the upper surface of a four-wheeled, angle iron cart. Screw jacks are rigidly attached to the cart near the wheels, in order that, after proper placement, the cart may be leveled, and fixed in position.

The analyzer power supply is housed in the cart, immediately beneath the analyzer plate. Holes are cut in the surface plate, one beneath each analyzer plate. Electrical connections between the power supply and the analyzer plates are made through these holes. Lucite bushings are used to insulate the high voltage connectors from the grounded surface plate.

Appendix B

CALCULATION OF ANALYZER RESOLUTION

The calculation of the analyzer resolution is a simple, albeit tedious problem. A sample calculation is given below, in detail. The results of several such calculations are then tabulated. (See Table 4A.) Finally, these results are pictured in Figure 13, which is a graph of resolution, R, plotted against image slit width, w'', for various object slit widths, w'.

$M = -.634$

$w' = .635$ mm. (Condition under which our experiments were performed.)

$-Mw' = .402$ (Length of each component image.)

B = Length of component image in the image plane which is not eliminated by the image slit.

$D = (a/2)(1-M)q = (40.094)(25.4)(1.634)q/2 = 832.104\ q$ (mm.)

= Displacement of component image

First make a table showing D and the upper and lower limits

of the component images, as a function of q. (See Table 1A.) Next tabulate B vs. q for various values of w", and graph these results. (See Table 2A and Figure 12.)

For each value of w", we get a discontinuous curve, consisting of a straight line of slope, m, and a horizontal line. The only exception occurs when w" = -Mw', in which case the curve is simply the line of slope, m. If w" is less than -Mw', the horizontal line will have the ordinate, B = w". If w" is greater than -Mw', the horizontal line will have the ordinate, -Mw'. For a constant object slit width, w', the slope, m, remains fixed, independent of the image slit width, w".

The ordinate for each value of q represents the relative number of protons with a fractional deviation of energy, $e(V-V_o)/V_o$ = eq which pass through the image slit. Therefore, the area, A, bounded by each curve, w", the B axis, and the q axis, is a measure of the total number of protons passing through the image slit when its width is w".

For the special case in which the proton distribution is triangular, 75% of the protons passing through the image slit will have the absolute value of q, written /q/, $\leq$ /q'/, where /2q'/ is the full width of the distribution function at half maximum. Thus, it is convenient to arbitrarily select 75% as a figure of merit, and to define the resolution, R, for all proton distributions, as follows: R is the reciprocal of q', where q' is so chosen that 75% of the protons passing through the image slit have /q/ $\leq$ /q'/.

In order to determine the resolution for a given set of con-

ditions (object slit width equal w', and image slit width equal w"), it is simply necessary to plot the length of component image, B, against the fractional energy deviation, q, for the chosen values of w' and w". The area, A, beneath this curve is measured. This measures the total number of protons passing through the image slit under these conditions. The value q', such that the area bounded by the ordinate at q', the curve, and the B and q axes equals .75 A is then found. The resolution, R, equals 1/q'. In Figure 12, w' is fixed at .635 mm. A family of curves is then plotted for different values of w". The resolution is then determined for each w", and the results are plotted as one of the curves in Figure 13.

q	D(mm.)	Upper limit of image (mm.)	Lower limit of image (mm.)
0	0	.201	-.201
1/6480	.128	.329	-.073
1/3240	.257	.458	.056
1/2160	.385	.586	.184
1/1620	.514	.715	.313
1/1296	.642	.843	.441
1/1080	.770	.971	.569

Table 1A

w" (mm.)	B (mm.)						
	q = 0	q=1/6480	q=1/3240	q=1/2160	q=1/1620	q=1/1296	q=1/1080
.1	.1	.1	0	0	0	0	0
.2	.2	.173	.044	0	0	0	0
.3	.3	.223	.094	0	0	0	0
.402	.402	.274	.144	.017	0	0	0
.5	.402	.323	.194	.066	0	0	0
.6	.402	.373	.244	.116	0	0	0
.7	.402	.402	.294	.166	.037	0	0
.8	.402	.402	.344	.216	.087	0	0
.9	.402	.402	.394	.266	.137	.009	0
1.0	.402	.402	.402	.316	.187	.059	0
1.1	.402	.402	.402	.366	.237	.109	0
1.2	.402	.402	.402	.402	.287	.159	.031
1.3	.402	.402	.402	.402	.337	.209	.081
1.4	.402	.402	.402	.402	.387	.259	.131
1.5	.402	.402	.402	.402	.402	.309	.181

Table 2A

FIGURE 12

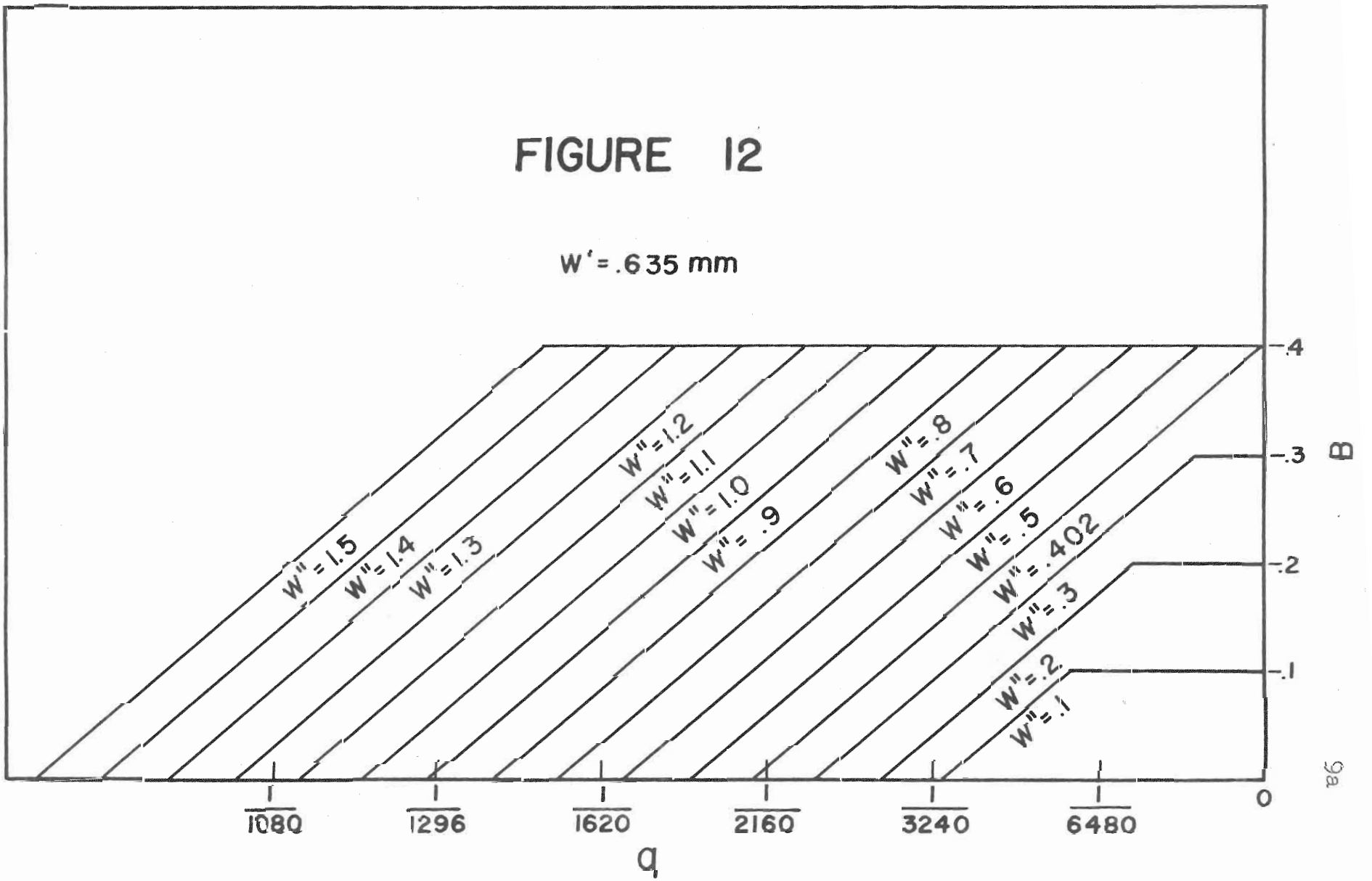
W' = .635 mm
W" = 1.5
W" = 1.4
W" = 1.3
W" = 1.2
W" = 1.1
W" = 1.0
W" = .9
W" = .8
W" = .7
W" = .6
W" = .5
W" = .402
W" = .3
W" = .2
W" = .1
.4
.3
.2
.1
B
1080
1296
1620
2160
3240
6480
0
q

w" (mm)	Relative Area	.75 A	R
.1	1250	937	5527
.2	2500	1875	5236
.3	3750	2810	4713
.402	4960	3720	4215
.5	6280	4710	3651
.6	7480	5610	3260
.7	8720	6540	2919
.8	9960	7470	2634
.9	11240	8430	2378
1.0	12480	9360	2165
1.1	13720	10290	1986
1.2	14960	11220	1834
1.3	16200	12150	1701
1.4	17440	13080	1583
1.5	18700	14025	1478

Table 3A

w"(mm)	w'=.2(mm) R	P	w'=.4(mm) R	P	w'=.635(mm) R	P	w'=1.00(mm) R	P
.1	19500	320	8610	780	5530	1250	3520	1960
.127	13290	* 510						
.2	10000	790	7300	1580	5240	2500	3520	3910
.254			6500	* 2040				
.3	7150	1190	5840	2400	4710	3750	3430	5780
.4	5550	1570	4910	3160	4220	* 4960	3200	7790
.5	4430	1980	4140	3980	3650	6280	2980	9695
.6	3680	2380	3580	4740	3260	7480	2775	11525
.634							2710	*12135
.7	3170	2760	3115	5560	2920	8720	2560	13530
.8	2770	3170	2750	6375	2630	9960	2370	15430
.9	2470	3550	2460	7140	2380	11240	2200	17330
1.0	2220	3960	2215	7960	2170	12480	2040	19240
1.1	2010	4360	2010	8770	1990	13720	1900	21140
1.2	1850	4740	1850	9540	1830	14960	1780	23040
1.3	1700	5150	1680	10350	1700	16200	1670	24940
1.4	1580	5550	1570	11170	1580	17440	1570	26840
1.5	1480	5930	1460	11930	1480	18700	1480	28750

*Triangular proton distribution function.

P = relative number of protons passing through image slit.

Table 4A

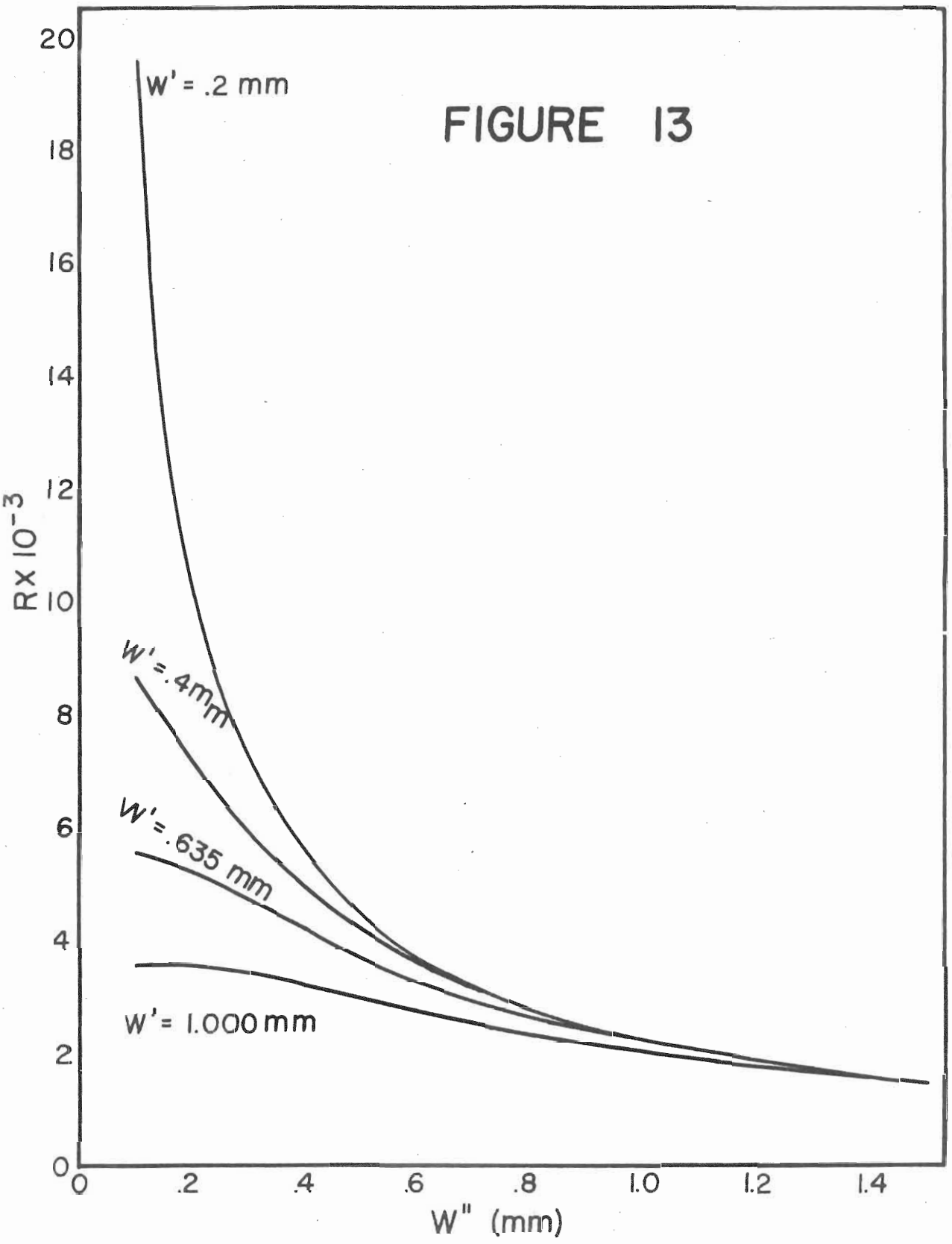
FIGURE 13
W' = .2 mm
W' = .4mm
W' = .635 mm
W' = 1.000 mm
R X 10⁻³
W" (mm)
0
2
4
6
8
10
12
14
16
18
20
.2
.4
.6
.8
1.0
1.2
1.4

Appendix C

POWER SUPPLY FOR ELECTROSTATIC ANALYZER

The analyzer power supply is designed to deliver a very steady potential to the analyzer plates. This is accomplished by means of a simple circuit consisting of two half-wave rectifiers and a resistance-capacitance filter. (See Figure 14.)

The high frequency of the generator, and the long time constant of the RC circuit, combine to reduce the ripple voltage to less than 1 part in 30,000. The capacitors have a resistance greater than 10,000 megohms, thus reducing leakage currents to negligible proportions. There are two resistor stacks, similarly constructed. Each consists of 27 one megohm and two 750 ohm resistors. All the resistors are wire-wound (manganin wire), made specially by the Shallcross Co., Collingdale, Pa., and accurate within 1%. In each stack, they are mounted in series, in a spiral, around a one-inch textolite rod, which extends in a horizontal plane, near one face of the chassis. Corona shields are spaced at equal intervals along the textolite column, such that

groups of three one megohm resistors are situated between every two shields. In addition to the three one megohm resistors in the group nearest to ground, there are two 750 ohm resistors in each stack. These resistors are connected to two outlets in the face of the chassis such that one furnishes the voltage tapped off at ± 750 ohms and the other at ± 1500 ohms, both relative to ground. Figure 6 which is a picture of the power supply, shows one resistor stack in the foreground.

Two 0-500 micro-ammeters are situated in the power supply chassis where they can be viewed through lucite windows. They read the current passing between each plate and ground. This current must be kept to a minimum, since there is the ever-present possibility of pitting the plates by repeated proton bombardment. In addition, any current between the plates and ground alters the plate potentials, thus decreasing the precision with which the energy of the proton beam is known. For example, suppose that the plate current fluctuates between 0 and 10 micro-amperes. The voltage drop between the plates and the top of the resistor stacks then varies between 0 and .81 volts. As shown in the section on apparatus, this implies an uncertainty in the proton energy of ± 90 volts. Should this current be permitted to reach 100 micro-amperes, the energy uncertainty would be approximately ± 900 volts.

As a protective "fuse," three 27,000 ohm, 1 watt resistors are mounted in series between each analyzer plate and the micro-ammeter in the circuit. Although it would be possible for a current surge to be large enough to burn out the meter without

harming the resistors, such an event rarely occurs. Ordinarily, the current remains well below 100 microamperes. When surges do occur, they are large enough to burn out the resistors almost instantaneously, thus opening the circuit and protecting both the analyzer plates and the meters. The efficacy of this arrangement is best attested to by the fact that these resistors have been burned out several times, with no observable deleterious effects on either the analyzer plates, or the micro-ammeters.

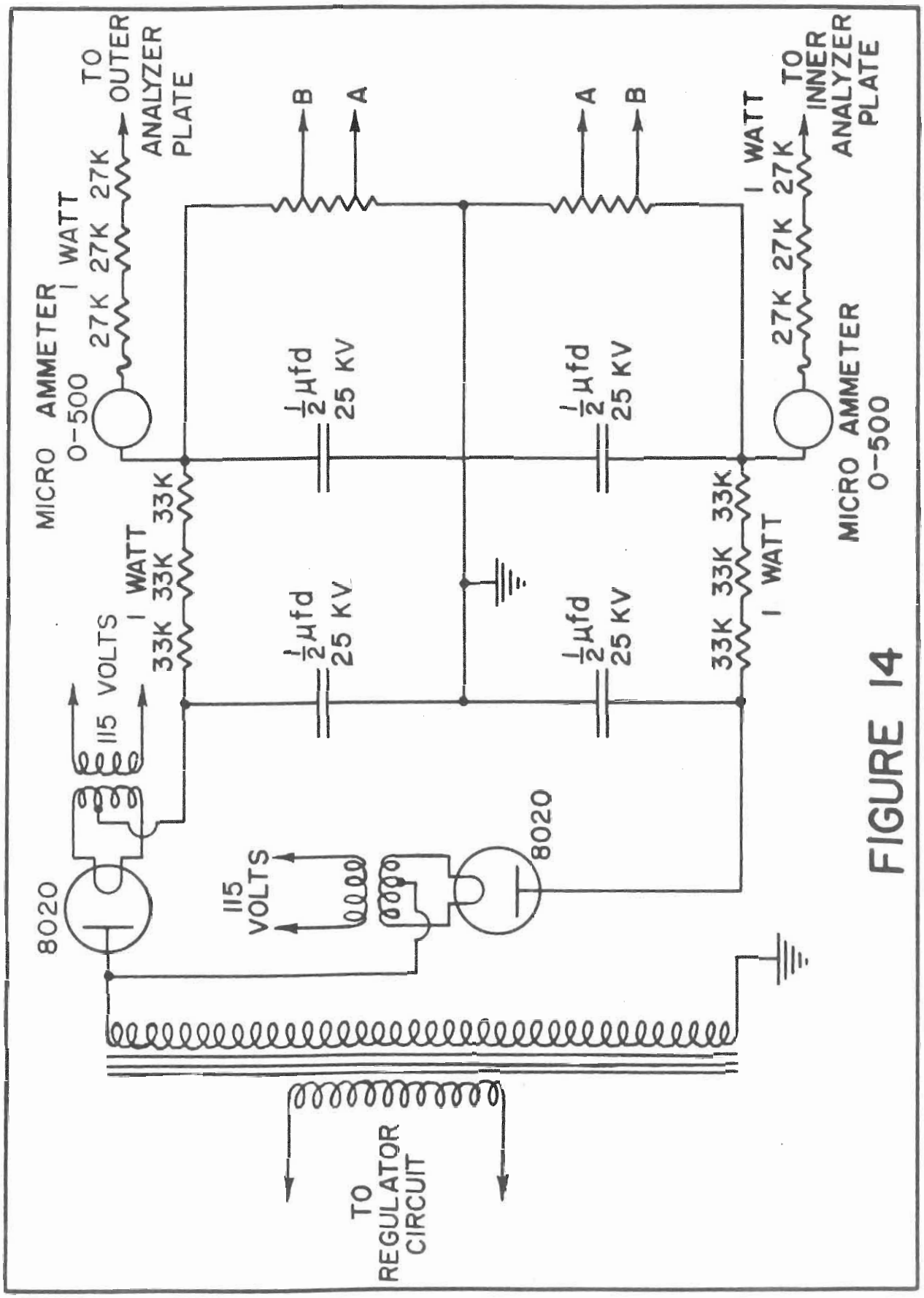
TO OUTER ANALYZER PLATE
TO INNER ANALYZER PLATE
MICRO AMMETER 0-500
MICRO AMMETER 0-500
1 WATT
27K 27K 27K
1 WATT
27K 27K 27K
B
A
A
B
1/2 μfd 25 KV
1/2 μfd 25 KV
1/2 μfd 25 KV
1/2 μfd 25 KV
33K 33K 33K
1 WATT
33K 33K 33K
1 WATT
115 VOLTS
115 VOLTS
8020
8020
TO REGULATOR CIRCUIT

FIGURE 14

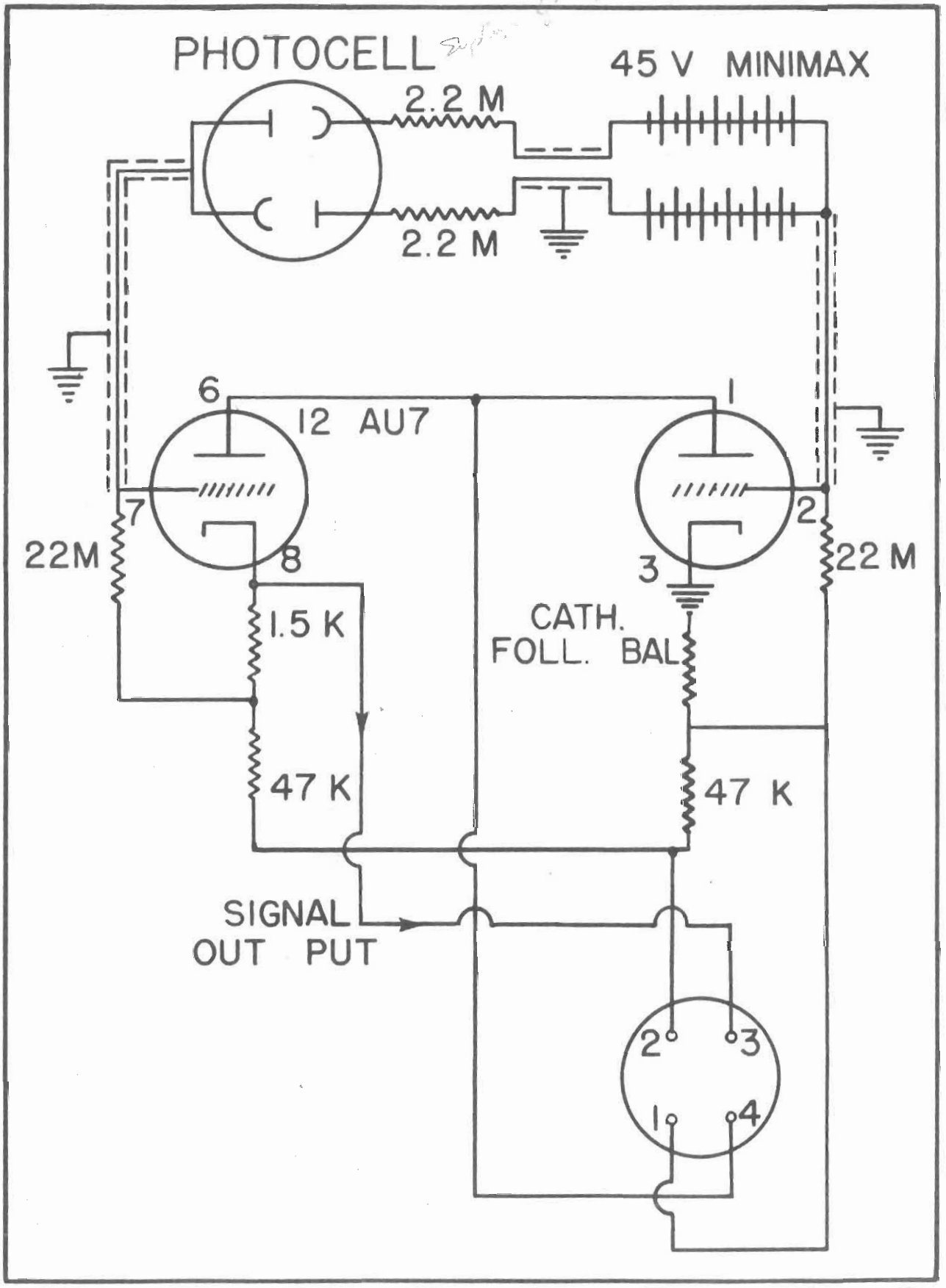
PHOTOCELL
45 V MINIMAX
2.2 M
2.2 M
6
12 AU7
1
7
2
22M
8
3
22 M
1.5 K
CATH.
FOLL. BAL
47 K
47 K
SIGNAL
OUT PUT
2
3
1
4

FIGURE 15

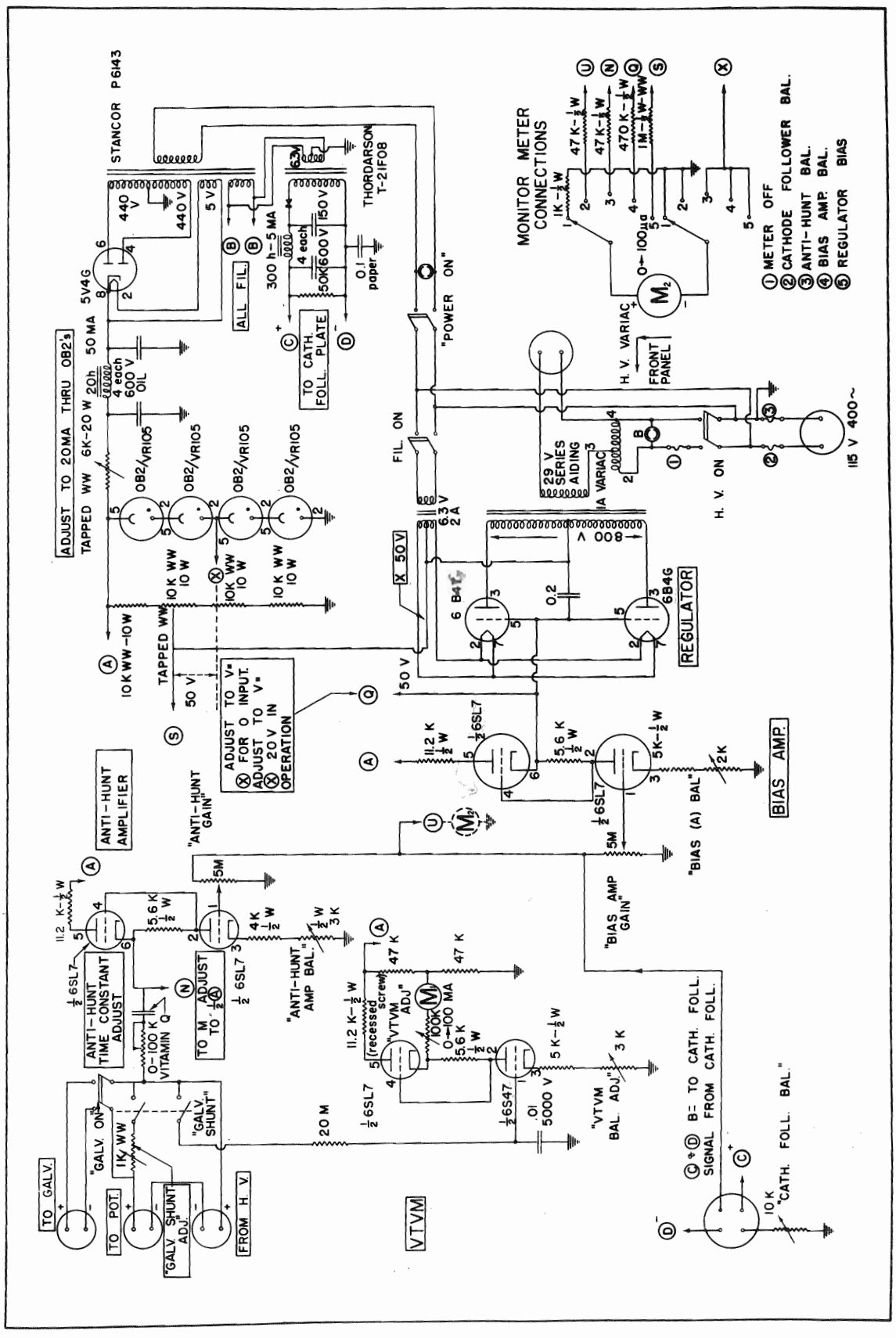
ADJUST TO 20MA THRU OB2's
TAPPED WW 6K-20 W
20h
50 MA
5V4G
STANCOR P6143
THORDARSON T-21F08
ALL FIL.
TO CATH. FOLL. PLATE
"POWER ON"
FIL. ON
MONITOR METER CONNECTIONS
1K-½W
47K-½W
470K-½W
1M-½W-WW
0-100μa
M2
H. V. VARIAC
FRONT PANEL
H. V. ON
115 V 400~
29 V SERIES AIDING
1A VARIAC
① METER OFF
② CATHODE FOLLOWER BAL.
③ ANTI-HUNT BAL.
④ BIAS AMP. BAL.
⑤ REGULATOR BIAS
OB2/VR105
4 each 600 V OIL
10K WW-10W
TAPPED WW
10K WW 10 W
50 V
ADJUST TO V- FOR 0 INPUT. ADJUST TO V- FOR 20 V IN OPERATION
X 50 V
6.3 V 2A
6 B4
6B4G
REGULATOR
ANTI-HUNT AMPLIFIER
"ANTI-HUNT GAIN"
11.2 K ½W
½6SL7
5.6 K ½W
5M
"BIAS AMP GAIN"
"BIAS (A) BAL"
2K
5K-½W
BIAS AMP.
ANTI-HUNT TIME CONSTANT ADJUST
0-100 K VITAMIN Q
TO M ADJUST TO ½
4K ½W
"ANTI-HUNT AMP BAL"
47 K
11.2 K-½W (recessed screw)
"VTVM ADJ"
0-100 MA
100K
5.6 K ½W
½6SL7
½6SU7
.01 5000 V
"VTVM BAL. ADJ"
3 K
20 M
"GALV SHUNT"
"GALV ON"
1K WW
"GALV SHUNT ADJ"
TO GALV.
TO POT.
FROM H. V.
VTVM
C & D B- TO CATH. FOLL. SIGNAL FROM CATH. FOLL.
10 K "CATH. FOLL. BAL."

FIGURE 16

Appendix D

ELECTROSTATIC ANALYZER POWER SUPPLY CONTROL CIRCUIT

The regulated output of the 400 cycle generator furnishes the primary voltage for the high voltage transformer in the analyzer power supply. However, this voltage first passes through a control circuit which compensates for any changes in the analyzer plate voltages by varying the transformer input voltage.

The action is as follows. (See Figures 14, 15, and 16.) First, assume that the power supply is in operation, and that the plates are at some high potentials, (of the order of plus and minus 10 kilovolts). Taps are provided in the power supply resistor stack such that voltages may be tapped off at 750 ohms or 1500 ohms on either side of ground. I.E. the voltage drop across either 1500 or 3000 ohms may be used. The negative side is connected to the negative of the output of a potentiometer. The positive end of this tapped voltage is fed to one side of a galvanometer coil. The positive output of the potentiometer is connected to the other side of the galvanometer coil. After

balancing, as long as the potentials of the analyzer plates remain fixed, the two ends of the galvanometer coil will be at the same potential. However, if for any reason the voltage of the analyzer plates changes, the tapped voltage will change proportionally, and an error signal will be applied to the galvanometer.

The galvanometer used is a standard type which has been modified slightly. A standard automobile stop light bulb has been substituted for that normally used with this instrument, in order to furnish more intense illumination. An aluminum surfaced equilateral glass prism has been glued to the center of the scale where the position of the mirror is customarily read. The prism is so positioned that the lower portion of the light beam may be observed on the scale. The remainder, and major portion, however, is reflected in a direction approximately parallel to the front of the instrument. Two type 927 phototubes are mounted within the galvanometer case, such that when the light is centered on the prism, they are equally illuminated by the light reflected to each side.

When the error signal is applied to the galvanometer coil, the mirror is deflected, and one of the phototubes receives more, and the other less, light than in the quiescent condition. In order to isolate the high impedance phototubes from the following amplifier grids, this signal is passed through a 12AU7 cathode follower. The cathode follower output is then used to change the grid voltage of two series-balanced 6SL7 amplifiers. The output of one of these amplifiers changes the grid bias of two 6B4G triodes. These tubes act as a variable load in the

secondary of a transformer, which furnishes the primary voltage to the high voltage transformer in the power supply. Thus, an increase in analyzer plate voltage leads, almost instantaneously to a decrease in input voltage, and vice versa.

In order to prevent the galvanometer light from oscillating back and forth due to these sudden changes, an anti-hunt circuit is included. As stated above, the cathode follower output is fed to the grid of a second 6SL7, also series-balanced. The output of this amplifier is passed through a Sprague Vitamin Q condenser and variable resistor in series. The time constant of this combination is such that its output is the differentiated error signal. This is then applied to that end of the galvanometer coil to which the tapped voltage is applied. Polarities are such that the signal effectively damps the oscillations of the galvanometer mirror.

In order that the circuit behave as described above, certain quiescent conditions must prevail. For convenience in making, and checking these conditions, a monitor meter, with five different connections is mounted on the face of the control panel. Its first position is simply "Off" and is used to zero the meter. Position 2 connects the cathode follower signal to ground through the meter. Positions 3, 4, and 5 connect the meter to a common point which is at a constant potential, 210 volts above ground. Position 3 connects the output of the anti-hunt amplifier with this point, through the meter. Position 4 connects the grids of the 6B4G's to the common point through the meter. Position 5 connects the center tap in the secondary of the transformer which

couples the 6B4G's with the high voltage transformer, and this point through the meter.

To start operations, the 400 cycle generator should be turned on, and run for at least fifteen minutes while the tubes are permitted to warm up. With the galvanometer light on, and centered on the prism, the cathode follower balance should be adjusted until the monitor meter reads zero in position two. The anti-hunt balance should next be adjusted until the monitor meter reads zero in position three. Next the bias amplifier balance should be adjusted until the meter reads approximately one quarter scale in position four. In position five, the monitor meter should read approximately half scale. This is a fixed reading, and any appreciable deviation indicates improper functioning of the circuit.

After the quiescent conditions have been set up, the monitor meter is left in position four, and the bias amplifier gain is turned up about half way. The beam limiting slits are closed, and the galvanometer and galvanometer shunt switches are put "on." The galvanometer shunt resistance is put at its minimum value. The electrostatic analyzer is now ready to be put into operation.

The potentiometer is set to the proper fraction of the high voltage desired. I.E. for a known proton voltage, V_o, the proper plate voltages, $-V'/2$ and $V'/2$, can be calculated. The potentiometer setting is then 1/36,000 or 1/18,000 of V', depending on whether the 1500 ohm or the 3000 ohm taps are being used. The potentiometer switch is then closed, and the vacuum tube volt-

meter (on the face of the control panel) reading is noted. The potentiometer is then disconnected, and the variac is turned up until approximately the same reading appears on the voltmeter. The potentiometer switch is now closed and locked, and we are comparing the reference voltage with the potentiometer output. However, any error signal is being shunted around the galvanometer coil. The shunt resistance is now slowly increased. The galvanometer light will start to move, its direction of motion depending upon the polarity of the error signal. At this point, one may set the bias amplifier gain. It should be turned up to that point where any observable change of the galvanometer light from its central position causes full scale deflection of the monitor meter when in position four.

The anti-hunt gain may also be set at this time. With the anti-hunt gain at zero, as the shunt resistance is slowly increased the galvanometer light will oscillate slowly about its central position. The anti-hunt gain should be increased gradually, until the oscillations cease. The gain should be turned up beyond this point until the oscillations occur again. This time it will be noted that the frequency of oscillation is quite high. The gain should then be decreased until these violent oscillations have just ceased. This is the optimum gain setting.

In practice, both bias amplifier and anti-hunt gains, after being properly set, require no further adjustment, unless some trouble develops in the control circuit. Thus, even after a period of weeks without being used, the analyzer may be put into

operation without touching these two controls.

Having properly adjusted the gains, if necessary, one continues to increase the shunt resistance. It is quite likely that the light will be deflected violently, and lost. If such is the case, the shunt resistance should be reduced immediately to its minimum value. The light may be centered again by flicking the galvanometer switch several times, being careful to leave it "on" before again attempting to remove the shunt. Loss of the light beam indicates that the variac setting is too far from that required for the given potentiometer voltage. The variac should be readjusted. (The direction may be learned with experience by noting in which direction the light beam was deflected.) This adjustment is quite coarse, and a very slight change in variac setting causes appreciable change in analyzer plate voltage.

After resetting the variac, one again attempts to increase the shunt resistance to its maximum value. It is possible to speed the process by quickly reducing this resistance each time the light beam starts to move, and readjusting the variac before the light has been lost. After succeeding in increasing the shunt resistance to its maximum value, without losing the light, one then throws the galvanometer shunt switch "off." As a precaution, to protect the galvanometer, one should turn the shunt resistance to its minimum value. With the switch off, this has no effect on the circuitry. However, should an error signal, which is strong enough to damage the suspension, be applied to the galvanometer coil, one can immediately afford some protection

by flicking the galvanometer shunt switch to "on."

The analyzer is now ready to "control" the proton beam. The beam limiting slits are opened to permit protons to enter the analyzer. The Van de Graaff magnet control is continually adjusted to maximize the proton beam impinging on the target, and to minimize the number of protons striking the analyzer plates.

Small adjustments in the energy of the proton beam are made simply by changing the potentiometer setting. The analyzer plate voltage adjusts itself to the proper value with no further changes required. If the energy change is to be large, it is accomplished by changing both the potentiometer and the variac settings.

BIBLIOGRAPHY

BIBLIOGRAPHY

(1) Blatt, John M. and Victor F. Weisskopf, Theoretical Nuclear Physics (John Wiley and Sons, New York, 1952) p. 317.

(2) Chadwick, J., Proc. Roy. Soc. London, A136, 692 (1932).

(3) de Broglie, le Prince-Ringuet, Thibaud, and La Tour, Comptes Rendus, 194, 1037 (1932).

(4) Dunning, J. R. and G. B. Pegram, Phys. Rev., 43, 497 (1933).

(5) Fermi, Amaldi, D'Agostino, Rasetti, and Segre, Proc. Roy. Soc., A146, 483 (1934).

(6) Amaldi, D'Agostino, Fermi, Pontecorvo, Rasetti, and Segre, Proc. Roy. Soc., A149, 522 (1935).

(7) Dunning, J. R., Phys. Rev. 45, 586 (1934).

(8) Bethe, H. A., Phys. Rev. 47, 747 (1935).

(9) Breit, G. and E. P. Wigner, Phys. Rev., 49, 519 (1936).

(10) Bethe, H. A. and G. Placzek, Phys. Rev., 51, 450 (1937).

(11) Kalckar, Oppenheimer, and Serber, Phys. Rev. 52, 273 (1937).

(12) Bethe, H. A., Revs. Mod. Phys., 9, 71 (1937).

(13) Kapur, P. L. and R. Peierls, Proc. Roy. Soc., 166, 277 (1938).

(14) Siegert, A. J. F., Phys. Rev., 56, 750 (1939).

(15) Wigner, E. P., Phys. Rev., 70, 15 (1946).

(16) Wigner, E. P., Phys. Rev., 70, 606 (1946).

(17) Bohr, N., Nature, 137, 344 (1936).

(18) Harkins, W. D., J. Am. Chem. Soc., 39, 856 (1917).

(19) Elsasser, W. M., J. Phys. et Radium, 4, 549 (1933).

(20) Elsasser, W. M., J. Phys. et Radium, 5, 389, 635 (1934).

(21) Mayer, M. G., Phys. Rev., 74, 235 (1948).

(22) Way, K., Phys. Rev., 75, 1448 (1949).

(23) Harvey, J. A., Phys. Rev., 81, 353 (1951).

(24) Berthelot, A., J. Phys. et Radium, 3, 17, 52 (1942).

(25) Perlman, Ghiorso, and Seaborg, Phys. Rev., 74, 1730 (1948).

(26) Pryce, M. H. L., Proc. Roy. Soc., A63, 692 (1950).

(27) Glueckauf, E., Proc. Roy. Soc., 61, 25 (1948).

(28) Hughes, D. J. and D. Sherman, Phys. Rev., 78, 632 (1950).

(29) Barschall, Bockelman, Peterson, and Adair, Phys. Rev., 76, 1146 (1949).

(30) Haxel, Jensen, and Suess, Phys. Rev., 75, 1766 (1949).

(31) Thesis of Robert E. Warren, University of Wisconsin, 1947.

(32) Thesis of John H. Gibbons, Duke University, 1954.

(33) Herzog, R., Z. fur Physik, 89, 447 (1934).

(34) Henkel, R. L. and B. Petree, Rev. Sci. Ins., 20, 729 (1949).

(35) Thesis of John H. Gibbons, Duke University, 1954.

(36) Merzbacher, E and B. Chern, unpublished.

(37) Hibdon, Muehlhause, Selove, and Woolf, Phys. Rev., 77, 730 (1950).

(38) Thesis of J. Reid Patterson, Duke University, 1954.

Biographical Sketch of

A. Louis Toller

Born:
December 2, 1917, Philadelphia, Pennsylvania.

Education:
Temple University, B. S. 1938.
Temple University, 1948-1950.
Duke University, 1950- .

Positions:
Graduate Assistant, Temple University, 1948-1950.
Research Assistant, Duke University, 1951-1954.

Memberships:
American Physical Society
Sigma Xi

Publication:
Total Neutron Cross Sections in the Kilovolt Region: Se, Br, Y, I, and Cs, Phys. Rev., 94, 774 (1954).